UNIVERSIDADE DE LISBOA
FACULDADE DE CIÊNCIAS
DEPARTAMENTO DE FÍSICA

Development of an active detector for radon detection in air

Soraia Sofia Clareu Elísio

Mestrado Integrado em Engenharia Física

Dissertação orientada por:
Prof. Doutor Luís Peralta

2019

Dedicated to my mother.

Acknowledgments

Quero agradecer em primeiro lugar ao Professor Luís Peralta pela orientação prestada, pela paciência, e pelo apoio total na elaboração deste trabalho. Aos profissionais José e Miguel do Laboratório de Instrumentação e Física Experimental de Partículas, pela disponibilidade e ajuda técnica, e à Professora Guiomar pelo suporte e amabilidade.

Agradeço também todo o apoio e motivação que me foi dado pela minha família. Em especial à minha querida mãe Maria, a mulher mais forte e determinada que conheço. Ao meu pai José e à avó Judite. Aos meus irmãos Miguel, Rafael e Luís, e às minhas irmãs Sara e Débora.

A todos os meus colegas e amigos que a vida me trouxe. João, Kamal, Sara e Rafael, obrigada pelo companheirismo durante todos estes anos académicos, obrigada pelas gargalhadas, pelos desabafos e por estarem sempre presentes. A todos os meus amigos de infância pela grande diferença que fizeram na minha vida. Betinha obrigada por me teres proporcionado os melhores momentos! A todos os meus amigos da residência Egas Moniz, por me terem acolhido, vocês são a minha segunda família. Um obrigado especial à minha querida Filomena, à Catarina e à Ana, por serem as melhores colegas de quarto em todos os aspetos.

Por fim um obrigado sincero ao meu amor. Sem ti esta fase da minha vida teria sido muito mais difícil. Agradeço a ti, Andrea por acreditares em mim, por me dares força para não desistir, pelas palavras de coragem, pelo teu amor incondicional e também pela comidinha!

Abstract

In this thesis, we developed and tested an active device for radon in air detection. It was intended to operate in pulse counting mode for real-time measurements without the need of an active gas pumping system. The prototype presented is relatively simple, low-cost and reproducible, made of inexpensive and easy to acquire components. We used as a sensor the commercial low-cost Si-PIN planar photodiode SLCD-61N5 with an area of 9.67×9.67 mm^2, sensitive to alpha particles. An Arduino UNO was attached to the electrical circuit of the device to count the logic pulses and connected to a computer to send and save the data. The initial prototype is comprised of a commercial light-tight metal box with $22.2 \times 14.5 \times 5.5$ cm^3 with lateral perforations where the gas enters by natural diffusion.

Electrical pulse signals corresponding to the hit of the alpha particles in the sensor, distinguishable from noise, were observed in a test using a $^{241}\mathrm{Am}$ source. Indeed, this showed an excellent response to alpha particles detection.

We performed three different experiments to estimate the order of magnitude of radon concentration using passive alpha-track CR-39, the commercial monitor Ramon 2.2 and a sodium iodide detector employing rocks sample from Nisa uranium mine as radon source.

A new alpha-track counting technique, using the free CellProfiler software, was further applied and tested to replace the visual counting method during the CR-39 test. From the comparison between the two techniques, deviations of 1-14% were obtained, which are quite satisfactory, demonstrating the feasibility of use for rapid and cheap analysis of alpha-track detectors.

We also performed simultaneous measurements in radon atmosphere to test the prototype comparing its performance with a commercial Geiger given as reference. The total number of counts was recorded in 10 minutes intervals. We observed an increase of the sensitivity response of the prototype for a higher reverse voltage applied to the photodiode.

We carried out the same test for a month, keeping a fixed voltage, in order to study the prototype's stability for long-term measurements. A positive high correlation was obtained.

As a future work on it, our study suggests the possibility of making a fully portable detector powered only by batteries and data recording on a memory card attached to the Arduino. This will allow operating in areas where the electricity supply is not stable. Furthermore, despite the ability of the prototype to detect the presence of radon in air calibration study are necessary in order to obtain exact concentrations values.

Keywords: radon detection in air, photodiode, electrostatic collection, low-cost monitor

Resumo alargado

A exposição à radiação ionizante proveniente de fontes naturais é contínua e inevitável para todos os organismos vivos. De acordo com a UNSCEAR o radão e os seus produtos de decaimento são, de entre as fontes naturais, os responsáveis por cerca de 42% da distribuição mundial de exposição à radiação ionizante junto à superfície da Terra.

O radão apresenta vários isótopos sendo o mais comum o $^{222}\mathrm{Rn}$, produto da série radioativa do $^{238}\mathrm{U}$ abundante na crosta terrestre. À temperatura ambiente o radão encontra-se no estado gasoso. A libertação do gás das rochas ocorre devido ao recuo dos átomos de radão resultante da desintegração do $^{226}\mathrm{Ra}$ via emissão de uma partícula alfa. O gás pode ser emanado para os interstícios entre sedimentos, para a água ou permanecer confinado nas rochas. O facto de ter um tempo de meia vida de cerca de 3,82 dias confere-lhe tempo suficiente para que se difunda através das rochas porosas até à atmosfera. O mecanismo de transporte dá-se principalmente por difusão devido à presença de gradientes de concentração no solo. Vários fatores como a porosidade da rocha circundante, permeabilidade, quantidade de água presente nos poros, e fatores atmosféricos como temperatura e pressão, afetam diretamente o mecanismo de transporte e impulsionam ou não um aumento do fluxo de radão para a atmosfera.

Quando edifícios são construídos sobre solos ricos em descendentes naturais do uranio, a probabilidade de entrada e confinamento deste gás nos pisos inferiores das casas é acrescida, caso medidas de mitigação não sejam aplicadas. As principais vias de entrada do gás são por fissuras existentes no pavimento e paredes e pelas juntas das tubagens, porém este gás também pode se apresentar na água de poços ou canalização. Por vezes materiais de construção provenientes de áreas ricas em uranio e seus descendentes também podem levar a um incremento da concentração de radão dentro das edificações. Elevadas concentrações de radão são encontradas em habitações pouco ventiladas, principalmente nas caves perto do solo. É necessário ainda referir que por vezes numa mesma área residencial nem todas as habitações apresentam os mesmos níveis de radão dada a grande variabilidade de fatores que influenciam o transporte.

O principal perigo é colocado essencialmente pela inalação dos descendentes radioativos sólidos polónios, chumbo e bismuto. Após o decaimento, estes produtos podem adquirir carga positiva, ou permanecer neutros. Quando electrostaticamente agregados a aerossóis, partículas suspensas de fumo ou poeiras adquirem grande mobilidade no ar podendo ser facilmente inalados. Devido a terem tempos de meia vida curtos estes podem ficar retidos no trato respiratório, depositando-se ao longo do mesmo. Após decaimento há libertação de partículas alfa altamente ionizantes que depositam toda a sua energia no tecido celular do epitélio pulmonar, sendo um fator incremental no risco de desenvolvimento de cancro do pulmão. Esta é considerada a segunda causa de cancro do pulmão depois do tabaco.

Como o gás radão não tem cor, cheiro ou sabor não é detetável pelos nossos sentidos. A única forma de

o detetar e quantificar é efetuando medições utilizando determinados dispositivos. A quantificação pode ser realizada diretamente da deteção de radão, indiretamente através dos seus descendentes, ou de uma mistura dos dois processos. A quantificação pode ser via deteção de partículas alfa, beta e/ou radiação gama, sendo o primeiro processo o mais comum. As técnicas de deteção de radão no ar podem ser subdivididas em técnica de recolha de amostras, de medição integrada no tempo e de medição contínua no tempo. Os dispositivos podem ainda ser caracterizados como sendo do tipo passivo ou ativo. A exalação do gás para a zona sensível do detetor pode ser ainda por difusão natural ou por bombeamento ativo.

O trabalho apresentado nesta tese de mestrado teve como principal objetivo o desenvolvimento e teste de um dispositivo para deteção de radão em ar. Pretendeu-se que funcionasse em modo contador de impulsos com medições em tempo real sem necessidade de bombeamento ativo de gás. O protótipo apresentado é relativamente simples, económico e reprodutível, composto por componentes baratos e de fácil aquisição.

Como sensor utilizou-se o fotodíodo planar Si-PIN comercial de baixo custo SLCD-61N5 com uma área sensível considerável de 9.67×9.67 mm^2, muito fino e portanto sensível a partículas alfa. O processamento de sinal implementado transforma os sinais originados da interação das partículas carregadas com o volume do sensor em impulsos elétricos. Esta cadeia é essencialmente constituída por um pré-amplificador, dois amplificadores lineares, um discriminador diferencial, um temporizador monoestável e por fim por um microprocessador Arduino UNO a funcionar como contador. O circuito elétrico foi desenhado em software Altium e as placas de circuito impresso fabricadas em laboratório seguindo um processo não industrial.

O protótipo inicial é constituído por uma caixa comercial metálica de tamanho $22.2 \times 14.5 \times 5.5$ cm^3 com perfurações laterais por onde o gás entra por difusão natural. As placas de circuito elétrico e o microprocessador foram instaladas no seu interior. É importante referir que o interior da caixa foi pintado com tinta preta do tipo mate e cartolinas colocadas em modo de barreira para prevenir que a luz atingisse o sensor.

De modo a testar a viabilidade do sistema para deteção de partículas alfa uma fonte radioativa de $^{241}\mathrm{Am}$ foi colocada em contacto com a área sensível do fotodíodo. O teste foi implementado dentro de uma caixa isolada à luz. Na presença de radiação foram observados sinais à saída do último andar amplificador com cerca de 400 mV a 1.8 V de amplitude. Na ausência de radiação sinais de 100 mV foram considerados provenientes de ruído eletrónico. Deste teste deu-se como estabelecido o desempenho para radiação alfa.

O processo de execução dos testes em condições laboratoriais para as várias experiências realizadas teve a mesma estrutura. Consistiu em uma caixa com fonte de radão e uma camara de testes onde os detetores foram posicionados, ligadas por um tubo por onde o gás se difundia.

A fonte de radão consiste em uma amostra de rochas proveniente da mina de urânio de Nisa em Portugal. Com o intuito de estimar a ordem de grandeza da concentração de radão produzida por estas rochas várias medições com vários detetores foram realizadas.

O primeiro método apresentado neste trabalho foi a exposição simultânea de detetores CR-39, com o monitor comercial Ramon 2.2 resultando em valores de concentração de radão de 3,4 kBq/m^3 e 2,3 kBq/m^3, respetivamente. Estas medições têm por base a deteção de partículas alfa provenientes dos decaimentos de $^{222}\mathrm{Rn}$, $^{218}\mathrm{Po}$ e $^{214}\mathrm{Po}$. O desvio encontrado é devido ao uso de um fator de calibração genérico, fornecido pelo fabricante dos CR-39, aplicado no cálculo dos valores de concentração.

Uma nova técnica de contagem de traços foi ainda aplicada e testada de modo a substituir a de contagem visual. Da comparação entre as duas técnicas obteve-se desvios de 1-14%, valores estes bastante satisfatórios que demonstram a viabilidade do uso para uma análise rápida e económica de detetores de traços.

Um outro método apresentado foi a exposição de detetor de iodeto de sódio de 2"$\times$2" resultando em um valor de concentração de radão de cerca de 100 kBq/m^3. Esta medição tem por base a deteção de radiação gama proveniente do decaimento do $^{214}\mathrm{Bi}$ e o cálculo de eficiência de deteção determinada com recurso a simulação PENELOPE. Considerou-se esta medida para estimar o tempo de exposição necessário do protótipo a diferentes níveis de radão em ar.

De modo a testar a viabilidade do sistema para deteção de radão em ar, este foi exposto na câmara de testes e os resultados confrontados com os de medições simultâneas de um Geiger comercial. O número de contagens total foi registado em intervalos de 10 minutos. Uma vez que os descendentes do radão adquirem carga positiva e dada a polarização inversa aplicada ao fotodíodo, existe um campo electroestático que atrai estes iões para a superfície sensível do sensor. Neste estudo observou-se um aumento da sensibilidade de resposta com o aumento da tensão inversa aplicada.

De modo a testar a estabilidade do protótipo desenvolvido, este foi deixado em exposição por cerca de um mês, comparando o seu desempenho com um Geiger comercial dado como referência. A resolução temporal dos dispositivos também foi de 10 minutos. Deste estudo obteve-se uma correlação alta positiva. Estimou-se ainda que para níveis de radão em ar de cerca de 100 Bq/m^3, o detetor deverá permanecer em exposição durante cerca de quatro dias a um dia, dado como razoáveis medições com incertezas associadas de 10% a 20% respectivamente.

Como trabalho futuro, sugerimos a possibilidade de tornar o detetor totalmente portátil alimentado apenas a pilhas e os dados registados num cartão de memória anexado ao Arduino. Isto irá permitir operar em áreas onde o fornecimento de eletricidade não é estável. É importante ainda salientar que o protótipo apesar de detetar a presença de radão no ar não apresenta medidas em concentração sendo necessário a realização de uma calibração no futuro.

Palavras-chave: deteção de radão em ar, fotodíodo, coleção eletrostática, monitor económico de radão

Contents

List of Tables

List of Figures

List of Acronyms and Abbreviations

FET Field-Effect Transistor.

GM Geiger Muller.

IAEA The International Atomic Energy Agency.

JFET Junction Gate Field-Effect Transistor.

MCA MultiChannel Analyzer.

NIM Nuclear Instrumentation Module.

PADC Polyallyl Diglycol Carbonate material also known as CR-39.

PCB Printed Circuit Board.

PENELOPE Penetration and ENErgy Loss of Positrons and Electrons.

PMT PhotoMultiplier Tube.

Si PIN Silicon Positive-Intrinsic-Negative diode.

TP Test Point.

UNSCEAR The United Nations Scientific Committee on the Effects of Atomic Radiation.

USB Universal Serial Bus.

Chapter 1

Introduction

1.1 Motivation

Radon, $^{222}\mathrm{Rn}$, is a radioactive gas that occurs naturally from the $^{238}\mathrm{U}$ decay chain. This element is present in rocks, soils and even in building materials that contain radon progenitor radionuclides. After its formation, the gas moves towards the atmosphere and tends to get into the buildings. Houses built in sites with a high concentration of radon can lead to an accumulation of this gas and consequently turning to be an important risk factor for human health.

The main concern is not due to the gas itself but it is due to the solid short half-life decay products produced as free ions. As a consequence of the strong probability for these ions to be electrostatically attached to aerosols, these clusters can remain in suspension, being easily inhaled and deposited in different regions of the respiratory tract.

Some of the radon progeny emit alpha particles that react strongly with matter depositing all their energy in a small volume in the lung tissue. Consequently, these constant irradiation damages the cells and can lead to the increase of probability of getting lung cancer.

The development of an active monitor will allow continuous evaluation of radon levels, and projecting the device with components with a fair price and easy to obtain will make it very accessible to handmade reproduction.

1.2 Objectives

The main objective of this work is the development and test of an active device for radon in air detection, with a low-cost commercial photodiode integrated as a sensor. The detector will be sensitive to alpha particles operating in pulse counting mode without discrimination in energy.

The associated electronics will also be designed and the printed circuit boards developed. The output

signal will be read by an Arduino UNO microprocessor that will present the results in counts.
In the last part, it is intended to test the prototype in a laboratory environment using a radon source and to compare the results with a Geiger counter over a certain time of exposure.

1.3 Overview of the dissertation

In chapter 2, we present general background information about the sources of ionizing radiation exposure and in more detail the natural radiation exposure from the radioactive gas radon. It is also present the main health effects of continuum exposure to this gas, and a description of techniques and devices commonly used to detect and measure the concentration of radon and its progeny in air.
In chapter 3, we present some preliminary experiments where we estimate the magnitude of radon concentration reached inside test chambers. The first is a coherence test between passive integrative CR-39 alpha-tracks detectors with a commercial semiconductor detector Ramon 2.2 is described. We also present a new method to count alpha-tracks by using free software CellProfiler. The last experiment is a reasonable suggestion to determine the concentration of radon in air using a sodium iodide detector.
In chapter 4, we describe the prototype development. We present the test implementation to prove the operability of the device using an alpha-emitting source $^{241}\mathrm{Am}$, the implementation of a study to see the effect of the variation of the reverse bias applied to the photodiode, and the implementation for the final long-time acquisition experiment.
In chapter 5, we present the results and its discussion of the experiments conducted.
Finally, in chapter 6, we summarize the experiments carried out in this work, and some recommendations for future work are given.

Chapter 2

Methods of radon detection

2.1 Sources of Radiation Exposure

2.1.1 Natural Radiation Exposures

Exposure to ionizing radiation from natural sources is continuous and inevitable for all living organisms. About 13% of the radiation origin can be from outer space, like cosmic rays, and 67% as terrestrial radionuclides from the Earths' crust present everywhere in the environment including in the human body [1, 2].

Cosmic radiation

High-energy particles from outer space are constantly reaching the Earth: protons and alpha particles (98%), and electrons (remaining 2%) [1]. These particles collide with the stable nuclei of atmospheric constituents, such as carbon, nitrogen, and oxygen, creating secondary particles such as protons, neutrons, pions, and lower-Z nuclei. Sequentially these secondary particles generate more particles producing a nucleonic cascade. The cosmic ray interactions also produce cosmogenic radionuclides, $^{3}\mathrm{H}$ (tritium), $^{7}\mathrm{Be}$, $^{14}\mathrm{C}$, and $^{22}\mathrm{Na}$.

Exposure to cosmic radiation is strongly dependent on altitude, decreasing in intensity with depth in the atmosphere (Figure 2.1). At ground level, about 70% of the contribution from cosmic rays is due to muons [1].

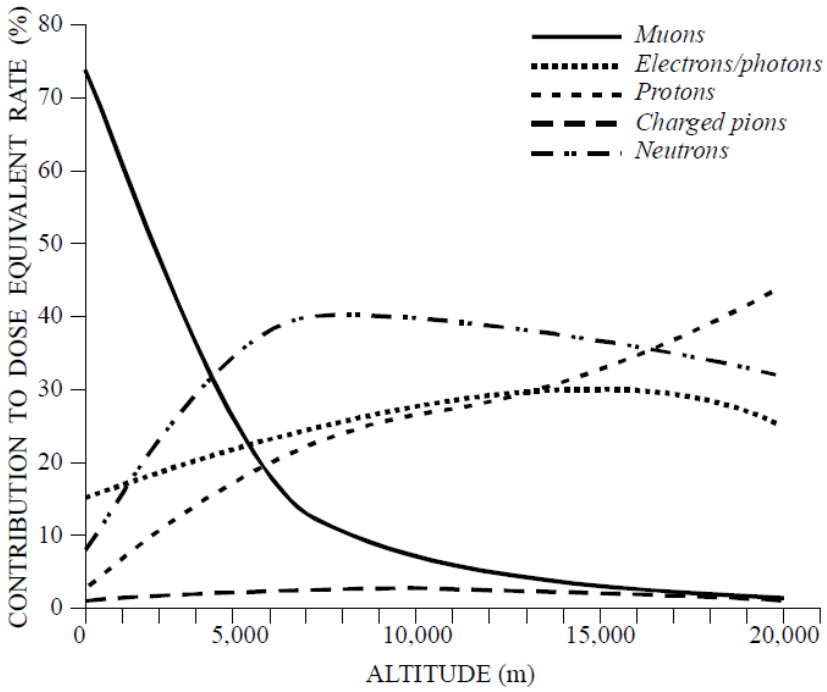

Figure 2.1: Contribution to dose equivalent rate with altitude dependence by the secondary cosmic ray constituents in the atmosphere [1].

Terrestrial radiation

Radionuclides of terrestrial origin, also known as primordial radionuclides, are present in the environment and in living organisms: potassium, uranium, thorium and their radioactive decay products, like radium, radon, and thoron. These radionuclides can be transferred to humans' body directly or through diet from air, soil, and water.

Irradiation from external sources is mainly due to gamma radiation emitted by the unstable ^{238}U, ^{232}Th series and ^{40}K (16%) [2].

Irradiation from internal sources is mainly due to alpha particles. It is caused by inhalation of the decay products of ^{238}U and ^{232}Th series aggregated with dust particles in the air, and by ingestion of ^{40}K and the decay products of ^{238}U and ^{232}Th series present in food and drinking water. The isotope ^{222}Rn and its decay products represent the dominant component of the internal exposure, of about 42% [1, 2].

2.1.2 Artificial Radiation Exposures

Besides natural radiation sources, there are activities and events involving radioactive materials that cause extra radiation exposures. The artificial sources represent about 20% of the exposure to ionizing radiation [2].

These activities are mainly related to production and use of radioisotopes in medicine and industry. In the past, events as the testing of nuclear weapons and one-off catastrophic events such as Chernobyl

and Fukushima accidents heavily contributed to accidental exposures. Emissions from nuclear power reactors, for generation of electricity, releasing and accumulation of nuclear waste in the environment also present a radiological risk [1].

2.2 Radon and Decay Products

According to UNSCEAR radon and its decay products are the most important contributors to human exposure from natural sources. Table 2.1 presents values of average annual effective radiation dose from natural sources.

Table 2.1: Values of worldwide average annual effective dose from natural sources. Evidence of the major contribution due to inhalation of radon [1].

Source	Worldwide average annual effective dose (mSv)	Typical range (mSv)
External exposure		
Cosmic Rays	0.4	0.3-1.0
Terrestrial gamma rays	0.5	0.3-0.6
Internal Exposure		
Inhalation (mainly radon)	1.2	0.2-10
Ingestion	0.3	0.2-0.8
Total	2.4	1-10

Characteristics

Radon is a naturally occurring gas. It is colorless, odourless, tasteless, almost chemically inert, and radioactive. It is the heaviest noble gas with the highest melting point, boiling point, critical temperature, and critical pressure. Radon is also soluble in cold water and such property increases the mobility of the gas in the environment [3].

Isotopes

There are 39 isotopes of radon ranging from $^{193}\mathrm{Rn}$ to $^{231}\mathrm{Rn}$ [4]. The three most common naturally occurring radon isotopes are: $^{222}\mathrm{Rn}$ (radon), $^{220}\mathrm{Rn}$ (thoron), and $^{219}\mathrm{Rn}$ (action) belonging to the series $^{238}\mathrm{U}$ (uranium), $^{232}\mathrm{Th}$ (thorium), and $^{235}\mathrm{U}$ (actanium) respectively [3].

The relative abundances of $^{238}\mathrm{U}$, $^{232}\mathrm{Th}$, and $^{235}\mathrm{U}$ are 99.27%, 99.98% and 0.72% respectively [5]. Thus, the action is significantly least abundant in nature. The half-lives of $^{222}\mathrm{Rn}$, $^{220}\mathrm{Rn}$ and $^{219}\mathrm{Rn}$ are 3.82 d, 55.6 s and 3.96 s, respectively [6]. Therefore radon has a half-life long enough for much of the gas to escape into the atmosphere. Thoron shows some chance to escape but with less radiological importance, and the action contribution is considered insignificant [1]. With this in mind, in our work, we will only consider as a result of the greater contribution the $^{222}\mathrm{Rn}$ isotope of the $^{238}\mathrm{U}$ series.

^{238}U decay chain and radon progeny

Figure 2.2 presents the radioactive decay serie of ^{238}U and the radionuclides involved, showing the radiation type of decay, as well as the characteristic energies and half-lifes.

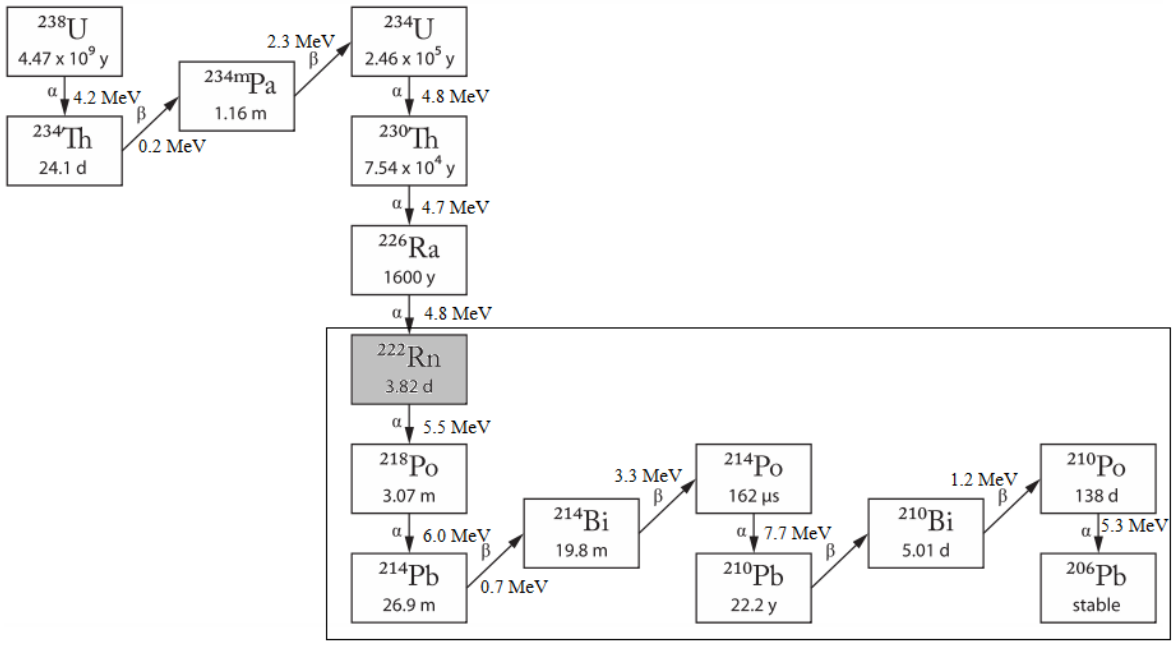

Figure 2.2: Uranium decay chain. Adapted from [7].

From the decay chain, notice that ^{222}Rn (gaseous) is a direct decay product of ^{226}Ra (solid). The following products are solid at room temperature, and the decay chain ends in the stable ^{206}Pb.

Radon source and transport process

As already mentioned, uranium is a naturally solid radioactive element present in several different geological environments. In 2016, IAEA classified the uranium deposits in fifteen major different types according to the geologic setting. These categories of uranium deposit can be intrusive (alaskite, granite, pegmatite, and monzonites rocks), granite-related (endogranitic, perigranitic), polymetallic iron-oxide breccia complex, etc [8, 9]. Because radon is a decay product of uranium it is expected to be more abundant in sites with the geological types presented above.

The release of radon from the rocks and sediments is due to alpha recoil process. When the decay occurs from the parent ^{226}Ra there is emission of an alpha particle and the radon atom created recoils escaping from the mineral. The radon atoms can go into the pore spaces between the grains, into water or remain trapped in the mineral, eventually decaying before the emanation (Figure 2.3) [3, 10].

After escape from the mineral, the radon gas presents greater mobility of movement. It tends to move towards the atmosphere through fractures and openings in rocks mainly by diffusion due to the presence of horizontal and vertical concentration gradients. The porosity of the surrounding rock, i.e. the dimen-

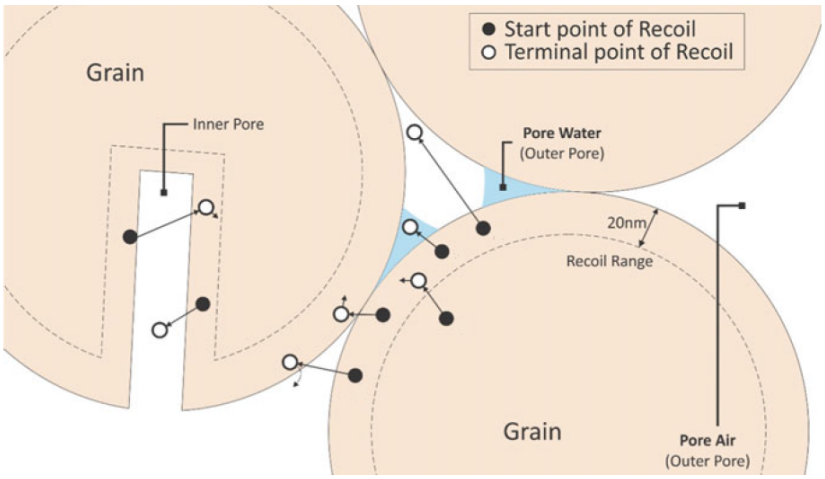

Figure 2.3: Representation of the recoil of radon atoms. Adapted from [10].

sion of the pore space that can be molecular interstices or large caves, the permeability, i.e. the way the pore spaces in the rocks are interconnected, and the soil moisture content, i.e. the amount of water present in the pore spaces, affect directly the transport mechanism. Factors as concentration of the parent radium in the site, barometric pressure, pressure-driven flow of air through the soil, wind, temperature, precipitation, snow or ice cover also have been shown to affect the radon movement to the atmosphere. Since this gas is soluble in cold water, so when occurs emanation of radon to spring water this gas has an easy way to propagate to further areas from the bedrock uranium site [1, 3, 10, 11].

It is well known that radon can also get into buildings before it decays, and when the houses are constructed in bedrock uranium areas with highly permeable soils, they may present high levels of radon. However, additional factors as the quality of the construction and mitigation actions affect the process of transport and thus the indoor radon levels. The movement of the gas into the houses is said similar to what happens in the underground. So, the most significant mechanism of transport is by diffusion, because of the presence of concentration gradients between the soil and the inside-house, or by pressure-driven flows of air from the ground beneath into the house driven by depressurization of the building. This flow-inducing mechanisms are mainly due to stack effects and were found some effects due to the wind, precipitation, and as well as barometric pressure variations. Earth-based building materials and domestic water derived from wells or at home from the tap can also be additional mechanisms of radon to entry inside the houses. Presence of radon in water can lead to release of the gas by evaporation and further inhalation [1, 3, 10].

Figure 2.4 shows the potential entry points for air-born radon into the houses. Basements are commonly the part of the house that appears to be most susceptible to high rates of radon entry. Once radon accumulated in houses, this turns to be an important risk factor for human health [11, 12].

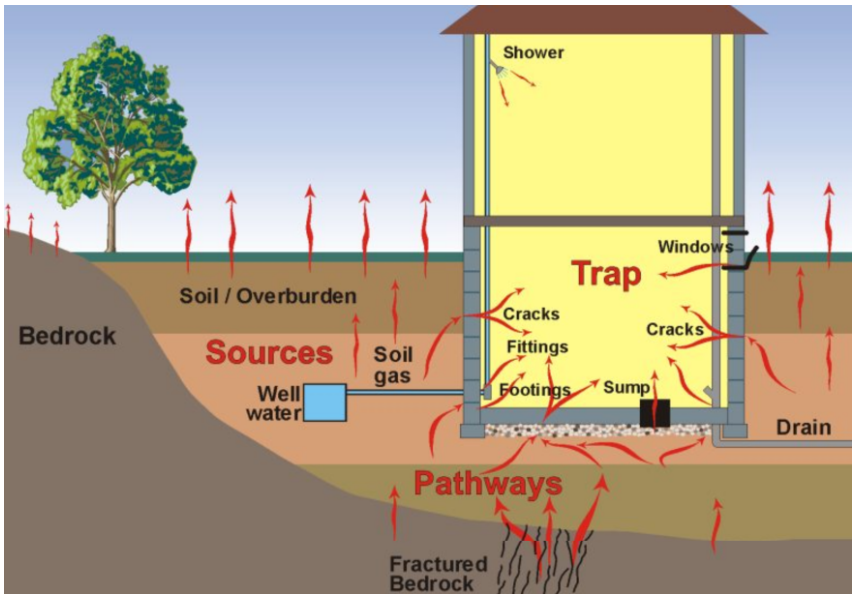

Figure 2.4: Representation of the potential entry points for radon migration into buildings. Adapted from http://www.dmf.unisalento.it/LaureeScientificheFisica/Download/ambiente/Lezione-Radon-GB.pdf.

2.3 Health Effects of Radon

In the past epidemiological studies of uranium miners had been performed and they demonstrated that accumulated exposure to radon and its decay products cause/increase lung cancer risk [13, 14]. They also suggest that something similar happens once radon accumulates inside buildings if mitigation actions are not applied [15]. It is also important to refer that the main concern is not due to the gas itself but due to the inhalation and deposition of the solid short half-life decay products in the lung [16–18].

When an atom of ^{218}Po is formed is initially known to be a positively charged ion. This is due to the stripping of orbital electrons by the emission of an alpha particle in the recoil motion. Studies suggest that about 88% of the polonium atoms are singly charged and that the remainder are neutral [19]. As a result of the positive charge, these atoms have a strong probability to be electrostatically attached to aerosols forming clusters. Aerosols are defined as suspension micro-sized particles such as dust or smoke, as well as water vapor. Figure 2.5 shows the process of the formation of clusters.

These clusters containing the radon progeny may remain in suspension being easily inhaled. The attached products can be deposited in different regions of the respiratory tract like the bronchi region or can be removed by mucociliary clearance. The remain unattached products may be deposited in the upper respiratory tract, and be removed by nasal deposition [3, 11].

The radon progeny have half-lives of the order of minutes/seconds and energies ranging from 5.3 MeV to 7.7 MeV. Since alpha particles interact strongly with matter they deposit all their energy in a very small volume of bronchial tissue. As a result of the cumulative dose of alpha radiation to the respiratory tract cells, they can be damaged leading to respiratory diseases increasing the possibility to develop lung

cancer.

Places with a high concentration of dust in the air, as well as smoke, provides a higher probability of attached nuclei, and therefore the increase of the risk [11].

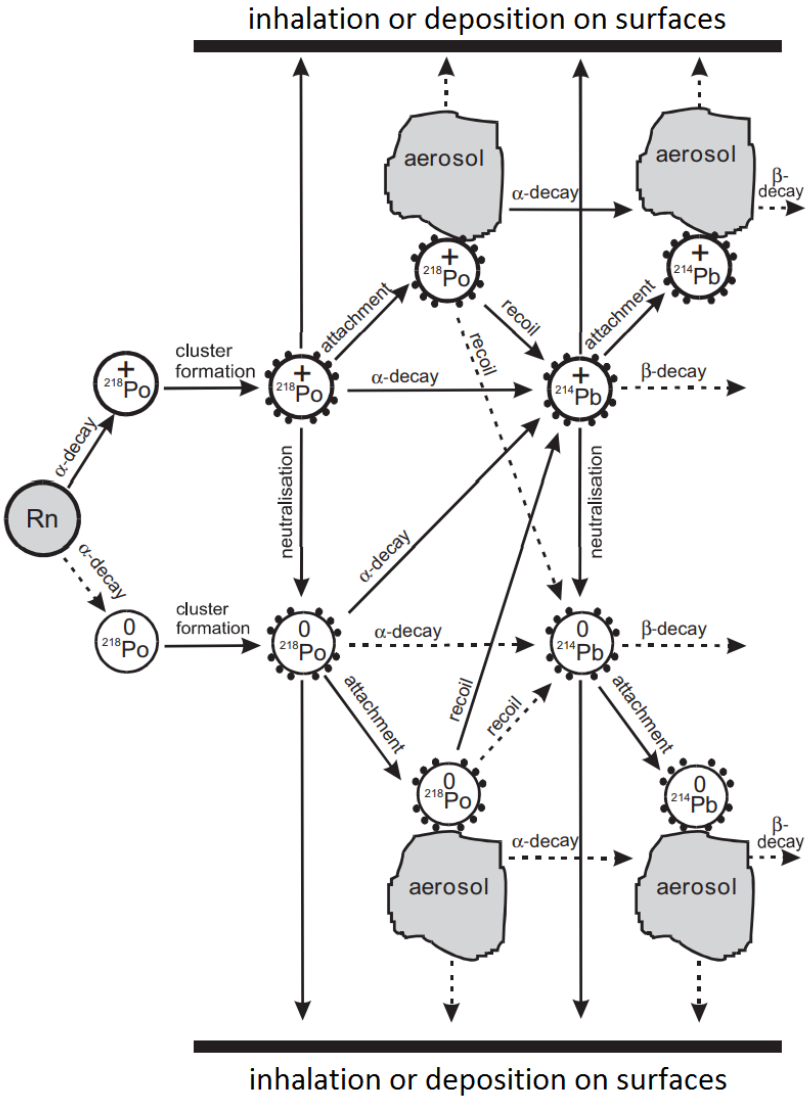

Figure 2.5: Schematic representation of the formation of radon daughter aerosols. Adapted from [19].

2.4 Radon Measurement in Air

It is necessary to use methods that ensure measurements reflect the actual exposure conditions during a certain period of interest. There is many different instruments and techniques available for the detection of ionizing radiation. Essentially the concept involves always a detection through the interaction of the charged particles or gamma-rays with the sensor material.

Radon and their descendants can be quantified through detection of emission of either alpha or beta particles or gamma radiation. Alpha particle detection is the most common way to quantify concentrations of radon since the background is usually smaller when compared to the detection of other types of radiation. However, due to their short range (just a few cms in air), the sensor must be positioned near the source [3].

The methods of detection of radon can be separated into three categories based on time resolution. These can be grab-sample, integrating and continuous techniques.

The grab-sample technique is the method that involves the measurement of radon from a discrete sample of air collected over less than 3 days at a single point in a study area. The advantage of using this technique is that is possible to make a large number of measurements in a short time.

The integrating technique is the method that involves integrated measurement of radon over a certain period of time. In this technique are used time-integrating detectors. These devices provide only a single value, which represents the average concentration in the study site, over typically a few days or a year of exposure. So, it is not possible to obtain information at the main time. The advantage of using these devices is that they are relatively inexpensive and accessible to users.

The continuous technique is the method that involves sampling and measurement of radon simultaneously over a long period. In this technique are used real-time detectors. These devices measure and record amounts of radon in air in real-time monitoring at regular intervals over a long period, providing constant information from the study site. The advantage of using this technique is the possibility to monitor the fluctuations in radon levels during the test period to make up to date informed decisions. Additionally, from continuous measurements, it is possible to record integrated results.

These devices may also be portable and are generally sensitive to the alpha particles which, when striking the sensor material, produces an electrical signal. They may include as well an integrated analysis system [10].

In addition, the devices may be further subdivided into two types: passive and active devices. Passive devices do not require power supply to operate, depend only on natural diffusion of the radon into the chamber and are less expensive. Active devices require power supply to operate, may involve either diffusion or pumping of air into the chamber and are generally more expensive. Also, radon detection is done either through direct methods of radon measurements, through indirect methods of radon progeny

measurements, or both. The last ones are based on the assumption of secular equilibrium between radon and its progeny [10, 11].

Factors as project costs, time resolution and sensitivity required, influence the decision to choose a technique and device.

In the following sections, we show some of the passive and active devices used to detect and measure radon.

2.4.1 Activated charcoal adsorption detector

Activated charcoal adsorption detector is a passive, time-integrated, inexpensive device to measure radon concentration in indoors.

This system consists of a small airtight metallic canister that contains about 50 to 100 g of granular activated carbon (Figure 2.6). To measure the radon in a site, the container is deployed and opened. Radon from surrounding air enters by diffusion into the canister and is adsorbed by the charcoal, being coupled to it, and the solid products attached. After the test period, the canister is sealed and sent to a laboratory for analysis. The analysis can be based on gamma decay from the radon progeny ($^{214}\mathrm{Pb}$ and $^{214}\mathrm{Bi}$), and measured using a scintillation sodium iodide crystal NaI(Tl) detector, or a semiconductor based detector. Sampling conditions such as humidity and temperature during the exposure time and the mixture of types of charcoal may influence the results.

This method is a good short-term indicator of radon contamination over small radon fluctuations. The collection time is about 1 to 7 days depending on the canister size. So long-term measurements are not representative with this method [3, 20].

Figure 2.6: Activated charcoal adsorption detector [21].

2.4.2 Electret ion chamber detector

Electret ion chamber detector (Figure 2.7) is a passive and time-integrated, inexpensive and lightweight method to measure radon concentration in indoors, used for both short-term (2 to 7 days) and long-term

tests (1 to 12 months) depending on the ion chamber design [20].

This system consists of an electrostatically teflon charged disk called electret placed inside a small chamber. This electret works both as a source of electric field and as a sensor. Radon from surrounding air enters by diffusion into the chamber. Alpha particles from the decay of radon and its progeny ionize the air molecules within the chamber. Ions move to the charged surface of the electret reducing its initial charge. This leads to a voltage drop over time that can be measured. Radon concentrations are then calculated from the electret voltage reduction applying a calibration factor.

Sampling conditions such as temperature and humidity during exposure may affect the results. These detectors also are not appropriate for use in sites with high radon concentrations. Measurements must be corrected for background due to gamma radiation [3, 18, 20].

Figure 2.7: Electret ion chamber detector. Taken from https://www.pembinatrails.ca.

2.4.3 Solid-state nuclear track detector

The passive solid-state nuclear track detector is a time-integrated detector. These detectors have been used in large-scale radon surveys due to their simplicity, lightweight and low-priced technique. Can also be placed either indoors or outdoors.

The sensitive part of the detector consist of a small piece of film generally made by poly-allyl-diglycol-carbonate (referred as PADC or CR-39), by cellulose nitrate (LR-115) or by polycarbonate substances (Makrofol). These films are usually encased in a small diffusion chamber covered with a lid. Radon from surrounding air enters by diffusion into the container through the gap between the lid and the chamber, of about 10 μm [22]. Figure 2.8 shows a schematic representation of the chamber and the diffusion pathway of the gas. Alpha particles from the decays strike the detector film producing damage marks, called tracks, with the size of less than 10 nm [10, 11, 20].

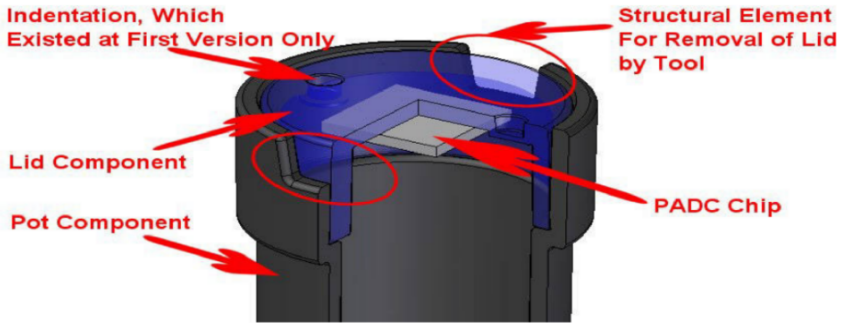

(a)

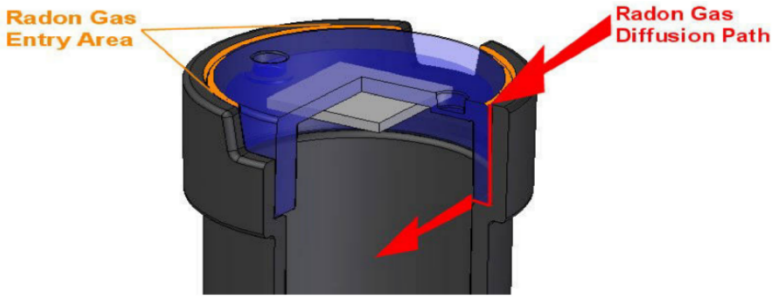

(b)

Figure 2.8: Representation of the CR-39 detector's chamber. (a) Inner structure and components. (b) Radon gas diffusion path into the chamber [22].

After exposure, the small chamber is sealed and sent to laboratory for analysis. The film is removed from the container and etched in a basic solution, usually sodium hydroxide (NaOH). This process increases the size of the alpha tracks making them visible by optical microscopy. The number of alpha tracks over a predetermined film area can be counted visually or using automated counting systems. Visual methods are laborious and highly user-dependent methods, so nowadays automated slide scanner counting systems such as Radosy's system have being used. However, these automated systems are much more expensive [22]. In this work, we present a cheap alternative to counting tracks using a free software.

The tracks density and the radon concentration in air are assumed to be in a relation of proportionality, thus the concentration of radon in air is calculated by using equation 2.1

$$c = k\frac{N - N_b}{tsM} \tag{2.1}$$

where, c is the radon concentration [Bq/m^3], N the number of tracks counted corresponding to the alpha-particle hits, N_b the number of tracks counted corresponding to the background radiation hits, s the film's area of study [cm^2], M the number of areas of study, t the exposure time [month], and k the calibration factor of the detector [Bq/m^{3}cm^{2}month] [23, 24].

The acquisition time required is usually at least 1 month and up to 1 year. It is not recommended for short-time measurement unless when placed in sites with high radon concentrations. Factors as humidity, temperature and background beta and gamma radiation, does not affect the measurements. It is also

important to refer that this detector should be always placed inside the container and that electrically conducting plastic containers are the ones that allow fewer measurements uncertainties [3, 11, 20].
The CR-39 films used in this work were produced by Intercast Europe. The general calibration factor of these films is k = 0.41 Bq/m^{3}cm^{2}month, which means that 1 track per cm^2 for 1 month of exposure results in having a radon concentration in air of 0.41 Bq/m^3 [25].

Figure 2.9: CR-39 detector and respective diffusion chambers.

2.4.4 Scintillation detector

Scintillation cell detectors can be either used for grab-sample, integrative or continuous techniques of radon and progeny measurement [10]. Thus, there are different designs of cells depending on the method chosen. The scintillating materials are then chosen for radon measurements through alpha particles detection or gamma-rays detection [20].
For alpha surveys are used the historically known Lucas cell (Figure 2.10). In general, the system consists of a cylindrical closed chamber with interior surfaces coated with the scintillating material silver-activated zinc sulfide ZnS(Ag) phosphor. At the bottom, the chamber has a transparent viewing window and on the top has a diffusive or a pumping system to collect the radon [10].
Radon from surrounding air goes into the chamber, and when the alpha particles emitted from the radioactive decays interact with the scintillating material, photons are emitted with wavelength in the visible range. At the bottom side of the cell a system that includes a photon detector, an amplifier and a pulse counter is coupled. The photon detector can be a photomultiplier tube (PMT) or a solid-state detector that converts the incident photons, that pass through the window, into an electrical signal. The pulse counter is usually a multichannel analyser (MCA) [10].
After being properly calibrated a calibration factor relates the number of counts for a period of time to the radon concentration [10].

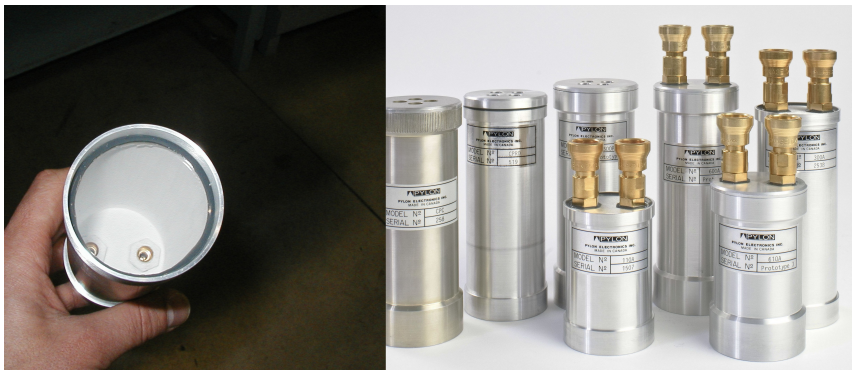

Figure 2.10: Scintillation cell detectors. Taken from https://pylonelectronics-radon.com.

For gamma radiation measurements is usually used scintillating sodium iodide crystals NaI(Tl) detectors. The gamma rays penetrate the detector aluminium housing and interact with the crystal material producing photons of visible light. These photons are then collected by a photomultiplier. Connected to the photo detector there is an amplifier and a pulse counter, like in the Lucas cell. The typical range of high voltage applied is from 900 V to 1000 V [10, 20].

2.4.5 Gas-filled detector

Gas-filled detectors can also be either used for grab-sample, integrative or continuous techniques of radon and progeny measurement [3]. There are three types of gas-filled detectors categorized as ionization chambers, proportional counters or Geiger-Muller (GM) counters that operate based on the same principle but differing the region of gas amplification in which they operate [20].

In general, the gas-filled detector system consists of a sealed or flow-through chamber. Sealed chambers are usually filled with a transfer gas such as nitrogen, nitrogen-hydrogen, argon, or helium at low pressure with a thin window through radiation goes [11]. Flow-through chambers are open to radon present in the air that can enter by diffusion or being actively pumped [3].

Inside the chamber, there are typically two electrodes an anode and a cathode. The alpha, beta particles or gamma rays emitted from the radioactive decays make the gas conductive by ionization, producing electron-ion pairs that are collected by the electrodes. To enable the collection of electron-ion pairs a high voltage must be applied. The electrical signal generated is after amplified and processed by an electronic associated [20].

The gas-filled detector used in this work was a commercial Geiger Muller counter (GM-10) from Black Cat Systems (Figure 2.11). The system consists of an enclosure with a Geiger Muller tube inside self-powered by the computers serial port. The radiation detected with this system is alpha, beta particles, and gamma radiation that enter through the sensing thin mica window. In this detector, the generated signal is independent of energy not being able to differentiate between types of radiation, so this device only functions as a simple counter of radiation-induced events. The counts were scored using the software

Rad provided by the GM-10 manufacturer [26**?**].

Figure 2.11: Geiger Muller (GM-10) from the Black Cat Systems [26].

2.4.6 Semiconductor detector

Like the two previous techniques, the devices based on photodiodes can also be either used for grab-sample, integrative or continuous measurements of radon. This technique usually incorporates an electrostatic collection of the positively ionized radon progeny [10, 11]. Depending on the operating conditions of the device, photodiode based detectors can be designed to detect either alpha, beta particles and/or gamma radiation. These devices can also be projected for spectroscopy or to work as a pulse counter. Photodiodes are made of semiconductor materials commonly silicon, mainly used for charged particle detection, or germanium mainly used for gamma radiation detection [20].

For radon measurements generally the system consists of a chamber within a silicon photodiode placed inside. Radon from surrounding air enters by diffusion or actively pumped into the chamber and the positively charged progeny are collected on the surface of the photodiode [27–33]. Then when the charged alpha particles, from the progeny decay, strike the surface of the photodiode its energy is absorbed along its track whose length is dependent on the energy of the incident particle. Electron/hole pairs are created in its path by coulomb interactions between the ionizing particle and the detection material. The electron/hole pairs are then separated by the electric field present in the photodiode junction in opposite directions. The photodiode operates in reverse bias mode, so electrons and holes migrate to the n-layer (cathode) and p-layer (anode), respectively, generating a flow of current in an external circuit. The produced charge is proportional to the energy of the particle incident (Figure 2.12) [34].

Photodiodes have a number of advantages: good quantum efficiency, small ionization energy, good energy resolution, good stability, good timing characteristics, variable thickness, compact size, low cost and simplicity of operation. However, electronic noise is a major problem due to the small signal amplitude [10, 34].

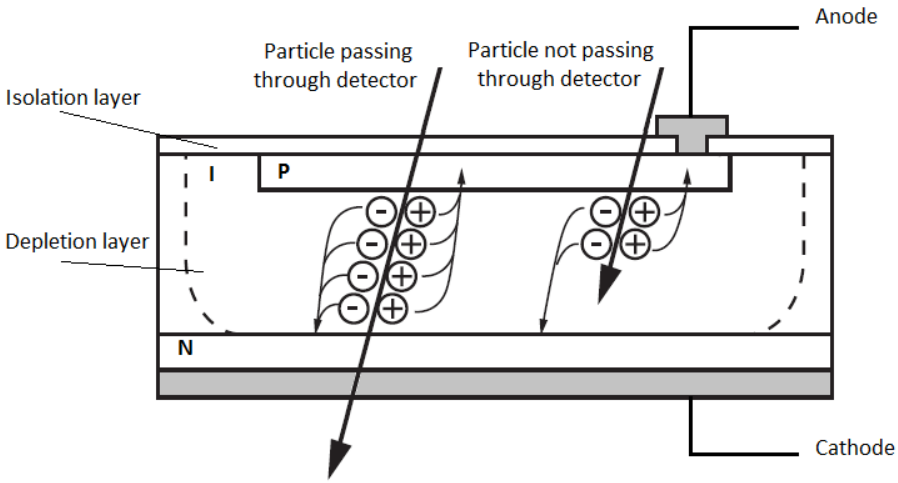

Figure 2.12: Schematic of a PIN photodiode cross section for charged particle detection. Image adapted from [35, 36].

In this work, we present a prototype for radon detection in air using the commercial low-cost silicon PIN photodiode SLCD-61N5 (Figure 2.13). Despite the desirable feature of superior energy resolution, a simpler approach of pulse counting was taken in this work once the goal was to build a simple and economic radon counter.

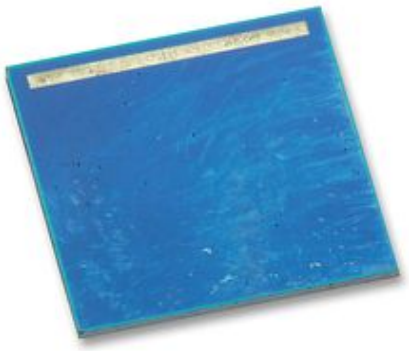

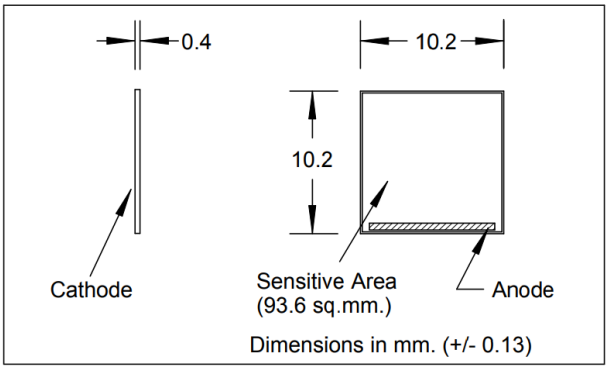

Electrical Characteristics (T_A=25°C unless otherwise noted)

Symbol	Parameter	Min	Typ	Max	Units	Test Conditions
I_{SC}	Short Circuit Current	2.5	4.0		mA	V_R=0V, Ee=25mW/cm^2 (1)
V_{OC}	Open Circuit Voltage		0.40		V	Ee=25mw/cm^2 (1)
I_D	Reverse Dark Current			3.3	μA	V_R=5V, Ee=0
C_J	Junction Capacitance		2.0		nF	V_R=0V, Ee=0, f=1MHz
S_λ	Spectral Sensitivity		0.55		A/W	λ=940nm
V_{BR}	Reverse Breakdown Voltage	20			V	I_R=100μA
λ_P	Maximum Sensitivity Wavelength		930		nm	
λ_R	Sensitivity Spectral Range	400		1100	nm	
$\theta_{1/2}$	Acceptance Half Angle		60		deg	(off center-line)

Specifications subject to change without notice 104114 REV 0

Notes: (1) Ee = light source @ 2854 °K

Figure 2.13: Characteristics of the commercial photodiode silicon PIN SLCD-61N5 used in this work.

We also used the integrative commercial semiconductor detector Ramon 2.2 (Figure 2.14) from Family Safety Products Inc. and calibrated by GT-Analytic SARL. This detector count the number of interactions of charged particles on the sensor over one hour and convert to radon concentration through a calibration factor, applying equation 2.2

$$c = \frac{N}{T} CF \tag{2.2}$$

where c is the radon concentration [Bq/m^3], N is the total number of pulses detected, T the number of cycles of measurement (one cycle is equal to one hour) and CF is the calibration factor. For the Ramon 2.2 used CF = 123 Bqh/m^3. This value was indicated by the calibration company [37].

The detector begins the measurements from the moment that is biased and has memory to save all the counts. The first result are only displayed on the monitor display after two days, and then every hour for the following measurements. The maximum of concentration that is possible to measure is 9999 Bq/m^3 [37].

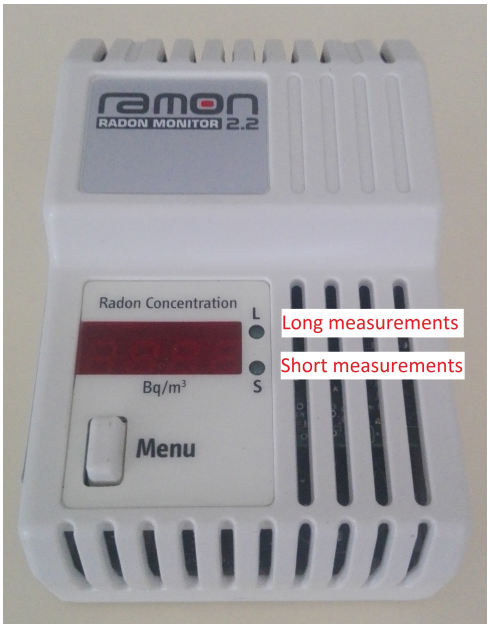

Figure 2.14: Commercial radon monitor Ramon 2.2. It is possible to set the monitor for short or long radon time exposure.

Chapter 3

Characterization of radon source

In this chapter, we present three different preliminary experiments where we estimate the order of magnitude of radon concentration achieved inside a test chamber employing rocks samples from Nisa uranium mine as radon source. Different techniques and detectors were used for this propose.

3.1 Passive CR-39 alpha track detectors versus commercial radon monitor Ramon 2.2

In this section, we present an inter-comparison of solid-state nuclear track CR-39 detectors with a commercial radon monitor Ramon 2.2. The integrated time was about 6 days. The data obtained from the CR-39 measurements were further used to test a new method to count alpha-tracks using the software CellProfiler. This is free and open source software designed to analyze images of biological samples [38]. One of the functionalities of the software is to count objects based on their size, which makes it favorable to use for our propose. Results obtained by using this software were compared with those obtained by visual counting.

3.1.1 Materials and methods

Passive CR-39 alpha-track detectors

The CR-39s used in this experiment were produced by Intercast Europe. They present two sensitive sides of 10×10 mm^2 initially protected against external agents by a thin film. Each film has its own serial number. These films were stored so as to avoid exposure to background radiation. For each one used, after removing the protective films, they were centered placed on the lid of each respective diffusion chamber and then placed inside the plastic test box (4.5 L) for irradiation (Figure 3.1).

After 6 days of exposure to radon, the CR-39 films were removed. In order to make visible the alpha-

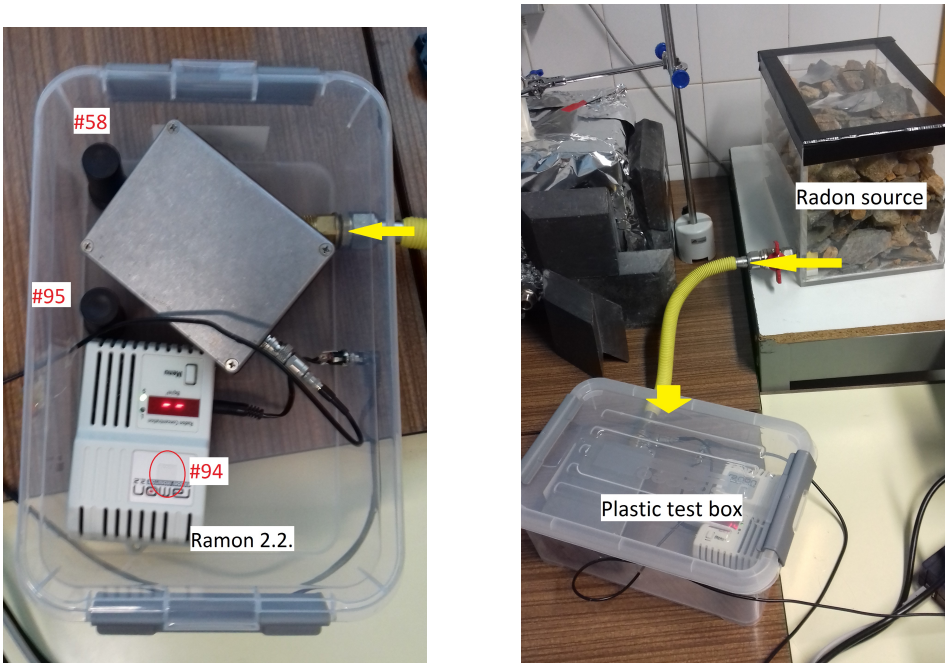

Figure 3.1: Experimental setup to estimate the radon concentration using passive CR-39 alpha track detectors and a commercial radon monitor. The results from the third detector are not presented in this study. The yellow arrows represents the radon gas flow movement.

particles tracks on the optical microscope, they were etched in a solution of sodium hydroxide (6 M NaOH solution) at 80-90 ^{o}C for 3 hours in a water bath (Figure 3.2(a)). A non-irradiated detector was also chemically etched so as to evaluate the contribution from the background radiation in storage conditions. After the chemical etching process, the CR-39 films were microscopic-readable. We used a Leybold optical microscope with a 100$\times$ magnification with a digital camera adapted to the ocular (Figure 3.2(b)). Four different areas of each film were photographed [24].

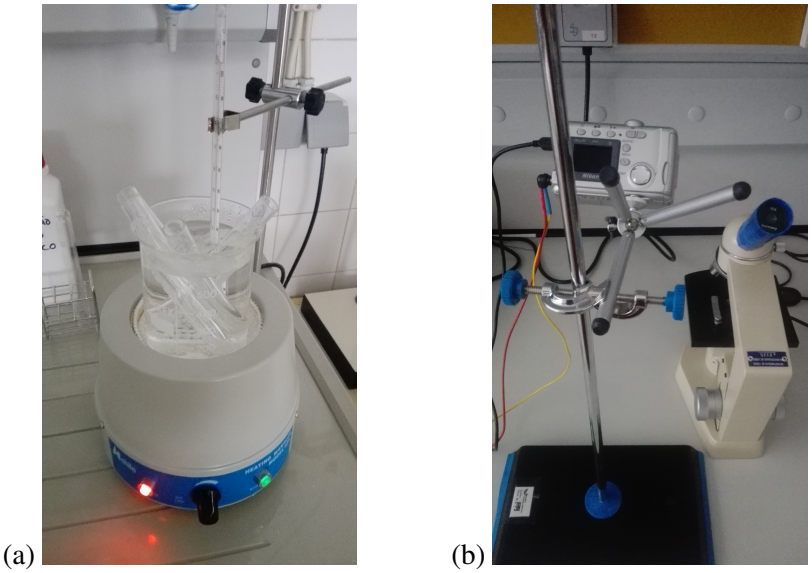

Figure 3.2: Experimental setup for (a) the chemical etching process and (b) for the photographs capture.

For each photograph, a specific area for study was set as 650$\times$650 pixel^2. A micrometer slide was used

to convert pixels to mm (1 pixel is equivalent to about 1.5 μm).

Finally, these images were grouped and imported into the CellProfiler software to perform a semiautomatic count of the alpha-tracks. Visual counting was also performed for comparison and control purposes. In short, we analyzed 16 photographs: 14 from the irradiated detectors (using visual and software counting method) and 4 from the non-irradiated detector (using only visual counting method).

In the software CellProfiler, we used the Identify-Primary-Objects module to identify the tracks. As the objects of interest are dark on a bright background, the Image-Math module was used to invert the images using the Invert operation. In the configurations, the input images were selected and the maximum and minimum limits of the typical diameter of the objects defined (in pixel units). Objects outside the diameter range were excluded but not the objects closed to the border of the images [39]. Through the Measure-Length tool, we measured the diameter of each track and the acceptance range was defined as 13-24 pixel (about 19-36 μm).

Radon monitor Ramon 2.2.

A Ramon 2.2 commercial radon monitor was also placed inside the plastic test box in continuing acquisition simultaneously with the passive CR-39 detectors. Before irradiation, the detector's internal memory was reset and the short-term measurement mode was selected. The results were read on the detector display and the uncertainty associated with the value calculated using a spreadsheet provided by the manufacturer.

3.1.2 Results and analysis

Figure 3.3 shows the microscopic images of alpha-tracks from the analysis of the CR-39 #94 detector. The diameter range of a track is 13-24 pixel, that is about 20-36 μm. Figure 3.4 shows the software's output resulting of the imported set of images from the respective former CR-39.

(a) 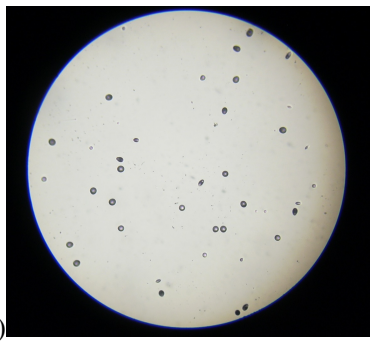 (b) 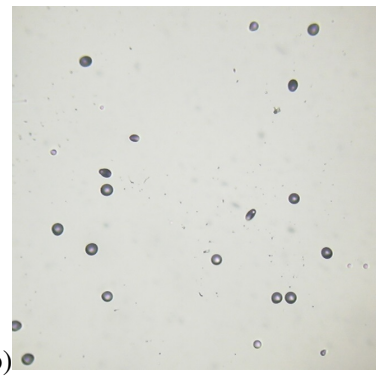 (c) 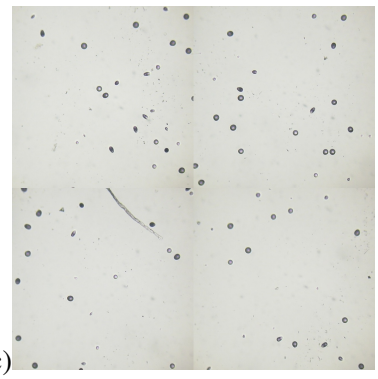

Figure 3.3: Microscopic images of alpha-tracks from the CR-39 #94 detector's analysis. (a) Typical image observed by optical microscope (100× magnification), after the etching process. (b) Cropped photograph with study area of 650×650 pixel^2 (about 0.9 mm^2). (c) Set of the four cropped photographs with 1300×1300 pixel^2 (about 3.6 mm^2) imported to the software.

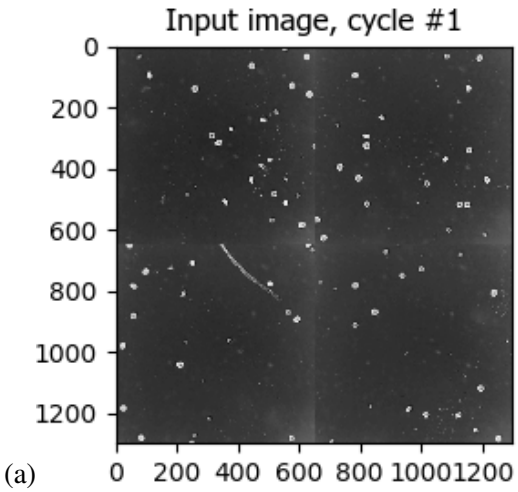

(a)

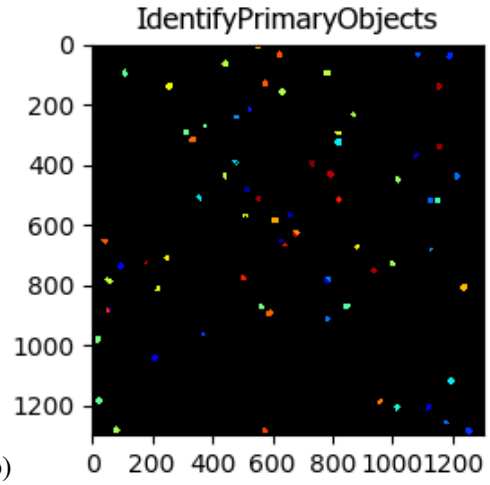

(b)

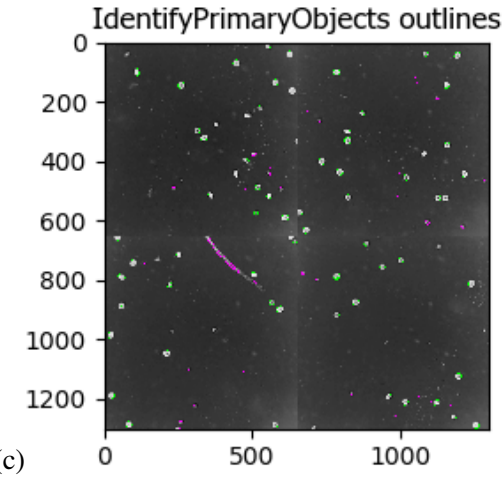

(c)

(d)

# of accepted objects	72
10th pctile diameter	15.4 pixels
Median diameter	19.8 pixels
90th pctile diameter	22.9 pixels
Area covered by objects	1.3 %
Thresholding filter size	1.0
Threshold	0.287
Declumping smoothing filter size	8.7
Maxima suppression size	9.1

Figure 3.4: CellProfiler software output. The size scales are in pixel. (a) Original image inverted. (b) Image with the identified objects dyed. (c) Image with the identified objects contoured with one of the two colors - green to the counted tracks and magenta to the excluded tracks due to their size. (c) Table with the number of the identified objects and some other features calculated/predefined by the software.

The radon concentration in the air was calculated using equation 2.1. The number of background tracks ($N_b = 2$), the studied area ($s \times M = 4 \times 0.00895$ cm^2), the exposure time ($t = 0.19$ month, about 6 days) and the calibration factor ($k = 0.41$) were kept constant.

Table 3.1 presents the values of radon concentration in the air calculated using the results by the visual counting method and by the semiautomatic counting method. The relative error percentage between the two methods is also presented.

Table 3.1: Radon concentration in the air calculated using the count results by applying the software CellProfiler and by visual counting. The respective total number of tracks and the relative error between the two methods is also presented.

CR-39	**N [track] Visual Inspection**	**c [Bq/m3] Visual Inspection**	**N [track] Software**	**c [Bq/m3] Software**	**Relative error [%]**
#58	58 ± 2	3296 ± 349	66 ± 8	3767 ± 592	14
#95	62 ± 2	3531 ± 371	65 ± 3	3708 ± 408	5
#94	71 ± 2	4061 ± 422	72 ± 1	4120 ± 416	1

Taking into account the uncertainties of each method, the results are in good agreement one with each other. However, it should be noted that the software is not totally rigorous in all situations. In some cases, there is an unrealistic counting of the tracks. It was noticed that occurs due to situations for instance when a single object is divided in two and counted twice, when artifacts as drops of water or dust are counted, and when the images have poor quality. In this study, the failures were mainly due to artifacts in the detectors and due to the size of some tracks (Figure 3.5).

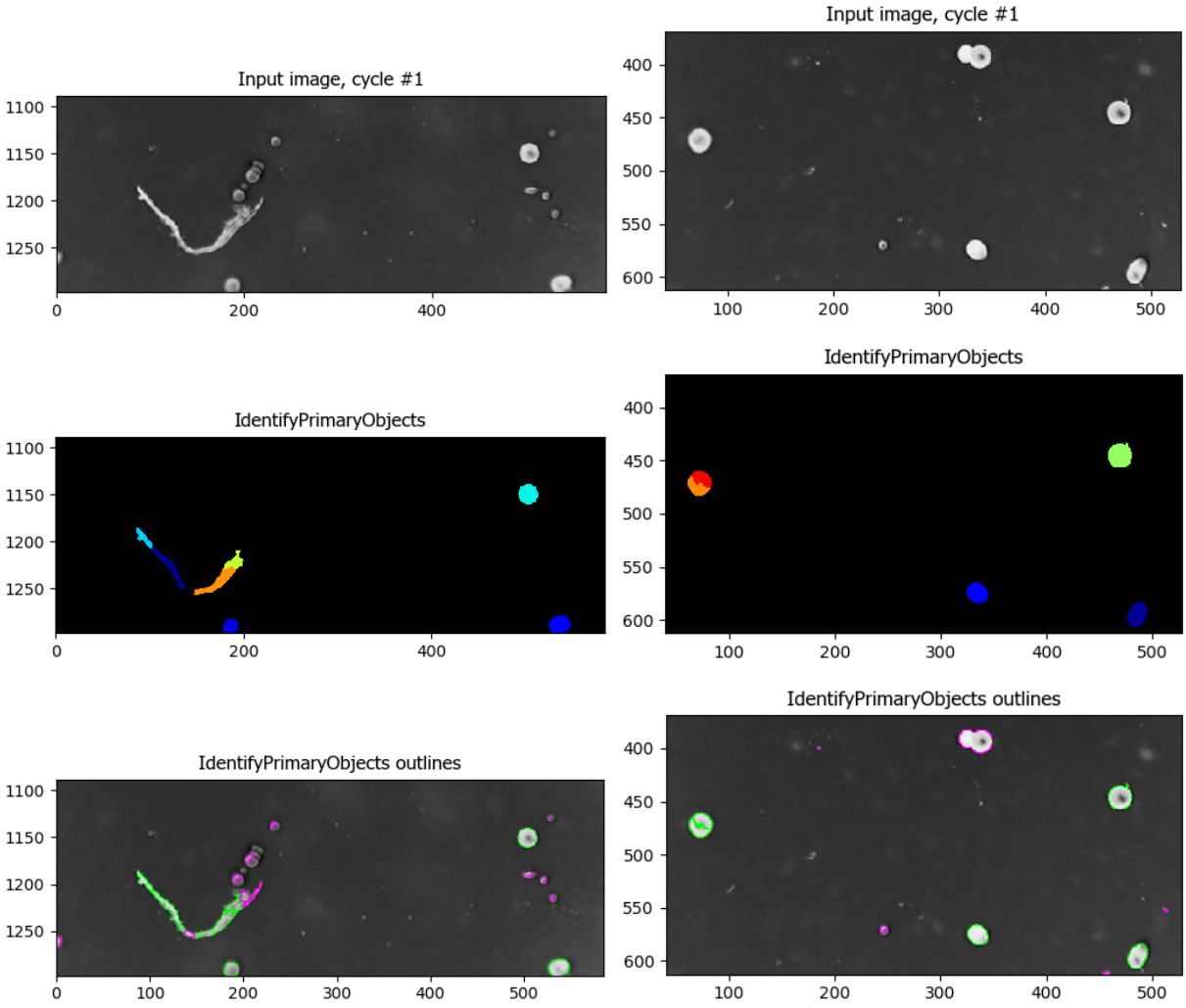

Figure 3.5: Cuts taken from analyzed photos that show some cases of presence of dust, division and failure identification of tracks that origins unrealistic counting. The size scales are in pixel.

The radon concentration read by the integrative semiconductor commercial detector Ramon 2.2 was (2300 ± 45) Bq/m^3.

Given the values of radon concentration resulting from the CR-39s analysis, using the visual counting method, we obtained deviations from the Ramon's value of about 43%, 54% and 77% corresponding to the detectors #58, #95 and #94, respectively. These analysis show reasonable results, except the value from the CR-39 #94. In fact, this higher deviation is possibly because this film was left in irradiation without the diffusion chamber.

It is important to take the methodology limitations into account. We note that may had been variations in temperature during the the chemical etching process, the presence of artifacts in the film's surface, the method of capturing the images was not adequate, and the calibration factor used in the calculations was a generic value provided by the manufacturer, not specific to the series of detectors in the experiment. Notwithstanding the limitations of the experimental methodology, this study was useful in the development of a new method to analyze CR-39 detectors.

3.2 NaI(Tl) scintillation detector

In this section, we present another methodology to estimate the radon concentration in air inside the test chamber employing gamma spectroscopy using a sodium iodide detector NaI(Tl).

3.2.1 Materials and methods

A NaI(Tl) scintillation detector 2"2" crystal from Canberra was used to estimate the radon concentration inside the test chamber. Coupled to the crystal there is a photomultiplier tube and a preamplifier. This detector is biased with 800 V, the signal amplified by a NIM Ortec 575A amplifier, and the events counted by a multi-channel analyser from Amptek. The detector is also enclosed in an aluminum case.
Figure 3.6 shows the experimental setup implemented for gamma spectroscopy. The detector is placed centered on the top of a 10 L test chamber. Two measurements were carried out, one for background radiation and other with a radon rich atmosphere.

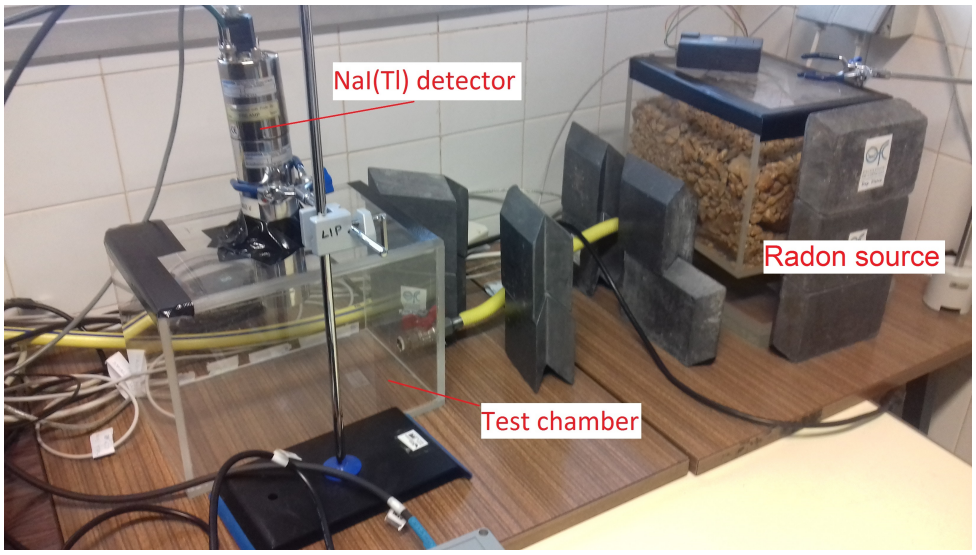

Figure 3.6: Experimental setup to estimate the radon concentration through gamma spectroscopy using a NaI(Tl) scintillation detector.

3.2.2 Results and analysis

As this detector is sensitive to gamma rays, it is possible to determine the average concentration of radon through the net areas under the peaks spectrum from ^{214}Pb and ^{214}Bi.

Thus the concentration of radon in air inside the test chamber can be determined by using equation 3.1

$$c = \frac{n_r/t_r - n_b/t_b}{\epsilon B V} \tag{3.1}$$

where, c is the radon concentration [Bq/m^3], n_r/t_r is the net area under the respective peak per the acquisition live time for radon [1/s], n_b/t_b is the net area under the respective peak per the acquisition live time for the background radiation [1/s], ϵ is the detector efficiency, B is the branching ratio for the respective isotope, and V the volume occupied by the radon gas [m^3].

The number of events is determined experimentally. In the spectrum, the 609 keV peak from ^{214}Bi was chosen for the measurement once this peak is well separated from the other contributions and has a high branching ratio of 46.1% (Figure 3.7).

The efficiency of the detector for the radionuclide peak energy can be computed by using Monte Carlo simulation through the code PENELOPE. This code performs simulations of electrons and photons transport in predefined materials and different three-dimensional geometries.

The volume occupied by the gas is the intern volume of the test chamber subtracted the detector's volume.

After about 16 hours of exposure to a rich radon atmosphere, the radon concentration inside the test chamber reached about 10^5 Bq/m^3.

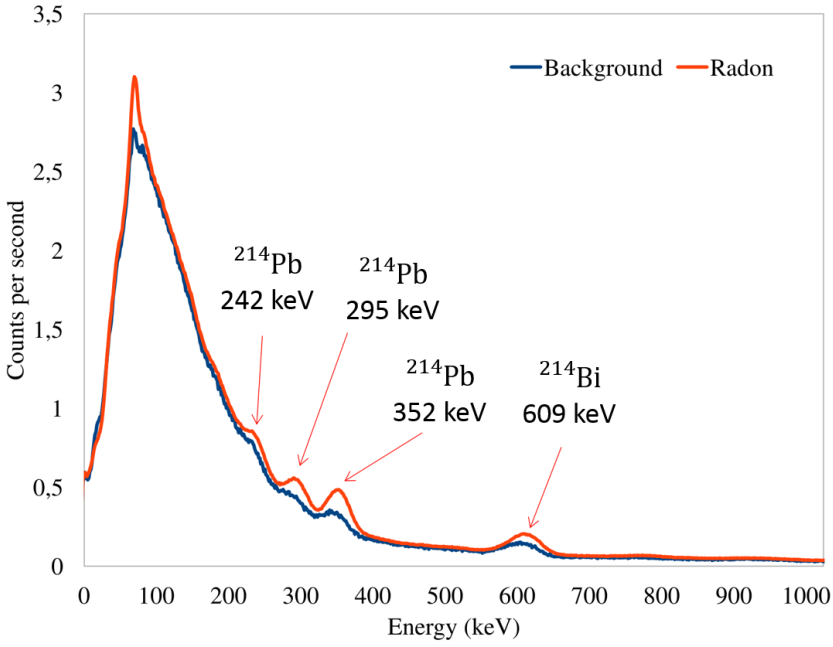

Figure 3.7: Gamma count rates results from the background and radon acquisitions using a sodium iodide detector.

Chapter 4

Prototype development

4.1 System design

The developed radon counter monitor is divided into three main parts: the sensor, the electrical signal chain, and the data acquisition system for pulse counting. Figure 4.1 presents a block diagram representative of the electronic system.

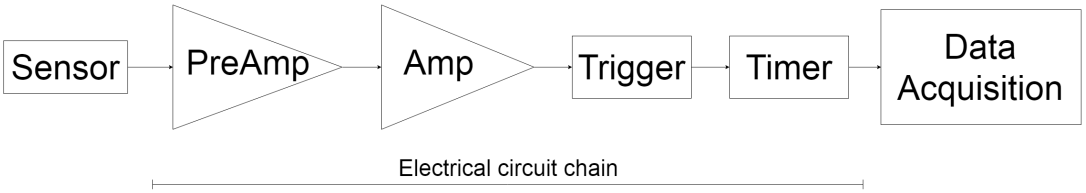

Figure 4.1: Schematic diagram of the electronic system.

A low-cost commercial photodiode silicon PIN Silonex SLCD-61N5 was used in this work as a sensor to detect alpha particles from the decay of radon and its progeny, under laboratory conditions. The active area of the photodiode is 9.67×9.67 mm^2, and the thickness is unknown.

A base was designed and built to support the photodiode, allowing its use in breadboards and/or perforated circuit boards. The dimension of this base is 18×11 mm^2. The photodiode has on its upper face a small metal contact, the anode, which was made connected with a wire to one set of pins of the support base. The back of the photodiode, the cathode, was welded to the same base and made connected to the other set of pins (Figure 4.2).

To achieve an efficient collection of charge created by the incident particles, a reverse external voltage was applied to the sensor. Thus, the anode of the sensor was made negative with respect to the cathode [34].

Figure 4.4 (1) shows the photodiode circuit implemented in this work. The load resistor R_1 limits the reverse voltage applied to the sensor junction, that should be lower than the breakdown voltage to avoid

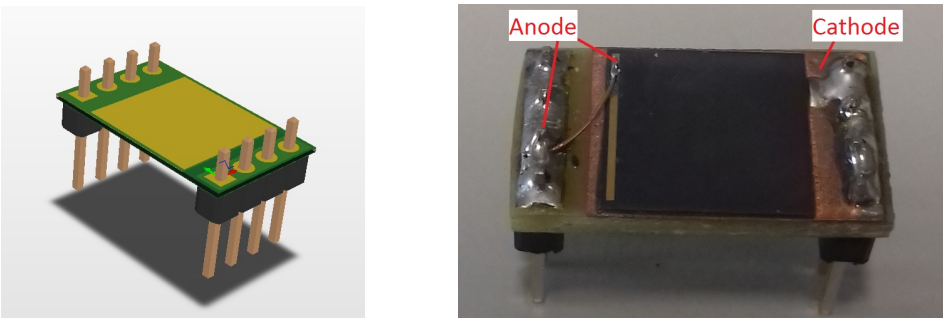

Figure 4.2: On the left a 3D design of the photodiode support base with the size of 18 × 11 mm2. On the right the commercial photodiode silicon PIN SLCD-61N5 welded to its base support.

increase of the leakage current and modification of the sensor proprieties. For the SLCD61N2 photodiode, the breakdown voltage is -20 V. The AC-coupling capacitor C_1, blocks DC bias signals.

As already mentioned, when a charged particle strikes the sensitive area of the sensor a small current is generated with amplitude proportional to the deposited energy. This current signal can be converted to a voltage signal using a transimpedance amplifier, commonly known as a charge-sensitive preamplifier. Since the photodiode polarity is reversed and the current signal enters on the inverse op-amp input, the output of the preamplifier will be a positive pulse. In order to have a conversion without significant degradation of the intrinsic signal-to-noise ratio, the preamplifier must be located as close as possible to the sensor and the op-amp used must have a FET (Field-Effect Transistor) input stage [34, 40, 41].

Figure 4.4 (2) shows the preamplifier circuit implemented in this work. The op-amp employed was a dual LF442 low power JFET input operational amplifier, with high gain bandwidth (1 MHz) and high slew rate (1 V/μs) [42].

The preamplifier output voltage, V, can be calculated through the equations 4.1 and 4.2

$$V = \frac{Q_d}{C_f} \tag{4.1}$$

$$Q_d = \frac{Ee \times 10^6}{\varepsilon} \tag{4.2}$$

where Q_d is the total release charge by the photodiode, C_f is the feedback capacitor (C_2 = 100 pF), E is the energy deposited in the photodiode in MeV, e is the charge of an electron ($e = 1.6 \times 10^{-19}$ C), ε is the average energy to produce an electron-hole pair in the photodiode junction (for silicon $\varepsilon = 3.62$ eV), and the 10^6 is to convert MeV to eV [41].

In a situation when the sensor is exposed to a radon rich atmosphere, alpha particles may be detected with maximum energy of 7.69 MeV, which corresponds to the decay of the ^{214}Po radon daughter. Thus, using equations 4.1 and 4.2, the maximum output signal should be of the order of magnitude of a few

mV.

In order to increase the amplitude of this signal from the mV range into the 1-10 V range, and to make possible accurate pulse detection, two stages of amplification were implemented. Figure 4.4 (3) shows the amplifier circuit implemented in this work. The resistors R_4 and R_6 set the voltage gain in the order of two thousand, being sufficient for the output signal to be in the desired range. The coupling between amplifiers is made by coupling capacitors also working as filters [40].

On the output of the amplifier, we placed a diode limiter circuit to limit the negative phase of the amplifier output signal.

With the aim of counting the pulses from radiation detector, these were converted into logic pulses by implementing a discriminator that produces a logic pulse, with a fixed height, when the input pulse is above a certain threshold. This allowed us to reject noise and small pulses from background radiation. The information that is recorded is only the presence or absence of a particle hitting the detector [34].

Figure 4.5 (1) shows the discriminator circuit implemented in this work. The chip employed was a single LM311 high-speed voltage differential comparator (response time of 165 ns) [43]. Due to the comparator input signal being noisy around the threshold value, a feedback resistor R_1 was implemented. The function of this resistor is to make the circuit have two input thresholds, instead of just one, preventing multiple triggering and consequently false pulse detection. This circuit is known as Schmitt Trigger [40]. Figure 4.3 (b) shows what happen when the signal is connected to the inverted input comparator. When

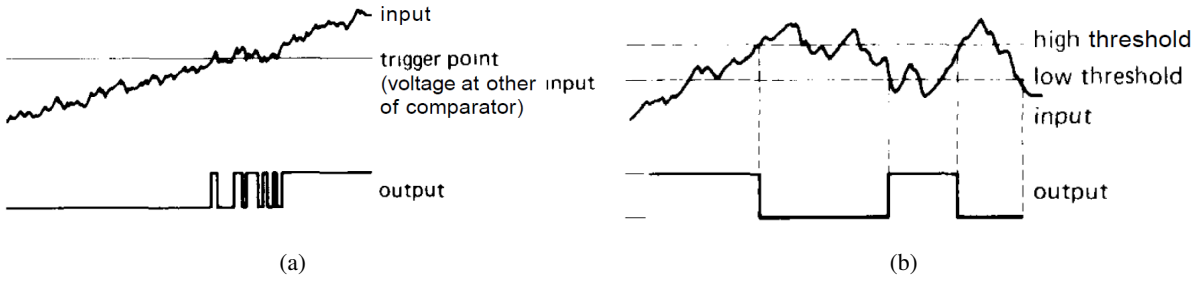

Figure 4.3: Representative schematic of trigger operation: (a) without feedback resistor and (b) with feedback resistor. Figure adapted from [40].

the input signal is below the high threshold value the output signal is held to a 'high' fixed value. When the input signal is above the chosen low threshold value the output signal is held to a 'low' fixed value. In order to have the output swing from ground to V_+ voltage, the pin 1 of the comparator chip was grounded and a pull-up resistor was placed at the chip's output [40].

The thresholds were experimentally adjusted taking into account the amplitude of noise and the pulse signals of greater amplitude observed on the oscilloscope. We deduced the equations 4.3 and 4.4 through

Kirchhoff's laws when the output is 0 V and V_+ respectively (V_+ = 9 V).

$$LowThreshold = \frac{R_1//R_3}{R_2 + R_1//R_3}V_+ \tag{4.3}$$

$$HighThreshold = \frac{R_3}{R_3 + R_1//R_2}V_+ \tag{4.4}$$

Finally, the last element of the circuit implemented was a timer working in inverse monostable configuration (as a trigger one-shot). The propose was to set a constant width for the pulses fed to the Arduino. Figure 4.5 (2) presents the timer implemented in this work. The chip employed was the common LM555 timer [44].

When the input signal is high the trigger is considered to be inactive, so the output signal is held near zero; when the input stage change from high to low the trigger is considered to be active and the output signal is held near the V_+ voltage (V_+ = 9 V). The time width of the output pulse is determined by the equation 4.5 [44]

$$T = 1.1R_5C_3 \tag{4.5}$$

The operating voltage of the microcontroller Arduino UNO is 5 V [45]. So, on the timer's output, we also placed a voltage divider where R_6 and R_7 with equal value connected in serie divide the signal by a fraction of 1/2.

4.2 Making the printed circuit boards

The design of the printed circuit boards was made by using the software Altium.

The circuit was designed to be small as possible and the components placed close as practical to minimize noise from the input capacitance caused by cabling, ground loops or radio-frequency pickups.

The layout design was printed to a film paper and its ink recorded to a board. We etched the copper in a solution and cleaned the PCB with water. In the end, we drilled the holes to afterward solder the components.

4.3 Testing the printed circuit boards

The printed circuit board (PCB) with the photodiode was placed inside a closed light-tight box. The polarization voltage applied was kept constant at -20V and the boards biased with +9/-9 V. To test the circuit we used an alpha-emitting $^{241}\mathrm{Am}$ source, with the most probable energy of 5.48 MeV [46]. Also,

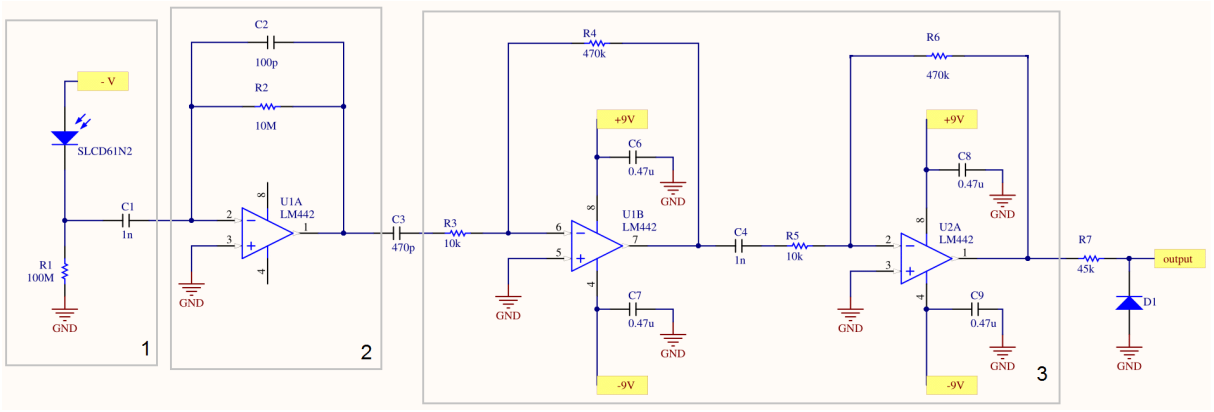

Figure 4.4: Schematic circuits layout of the (1) sensor, (2) the preamplifier, and (3) the amplifier. We used two LF442 Dual Low Power JFET input operational amplifiers [42].

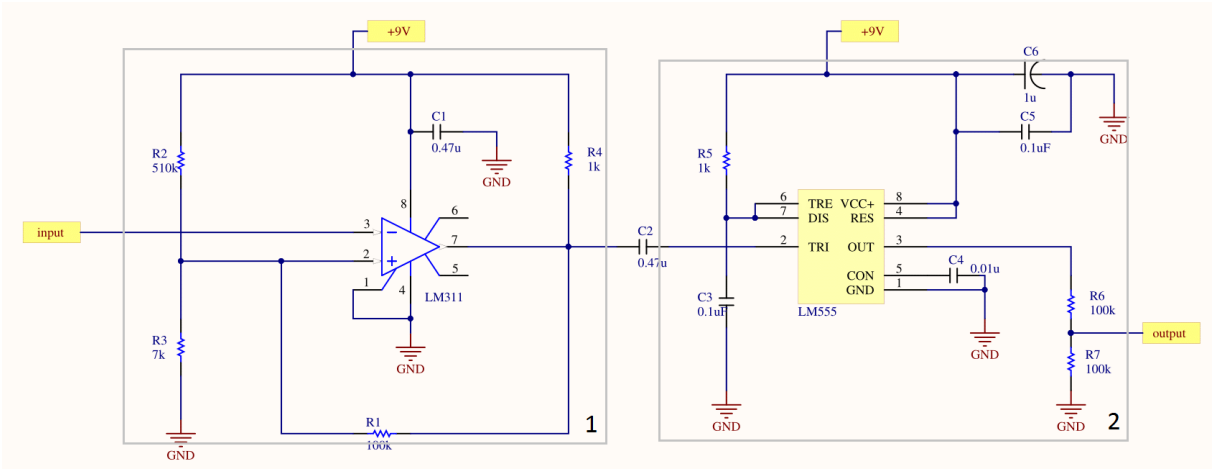

Figure 4.5: Schematic circuits layout of the (1) schmitt trigger and (2) of the timer. We used one LM311 voltage comparator designed for a very fast response and the monostable timer was implemented using the chip LM555 [43, 44].

note that alpha particles from the radon progeny have the most probable energy in the range of 5.5-7.7 MeV. With this in mind, the detection of particles from this source is sufficient to prove that the monitor detects radon. Figure 4.6 presents the implemented setup.

Figure 4.7 presents a block diagram representative of the electronic system with the indication of the three points chosen to read the signal. The test point number one (TP1) corresponds to the amplifier's output, the test point number two (TP2) to the trigger's output, and the test point number three (TP3) to the timer's output, which coincides with the Arduino's input.

4.4 Data acquisition with Arduino

The propose of this section is to count, store and display the number of digital pulses detected, corresponding to the presence of the radon in the air. To achieve this result a small code implemented in Arduino was developed.

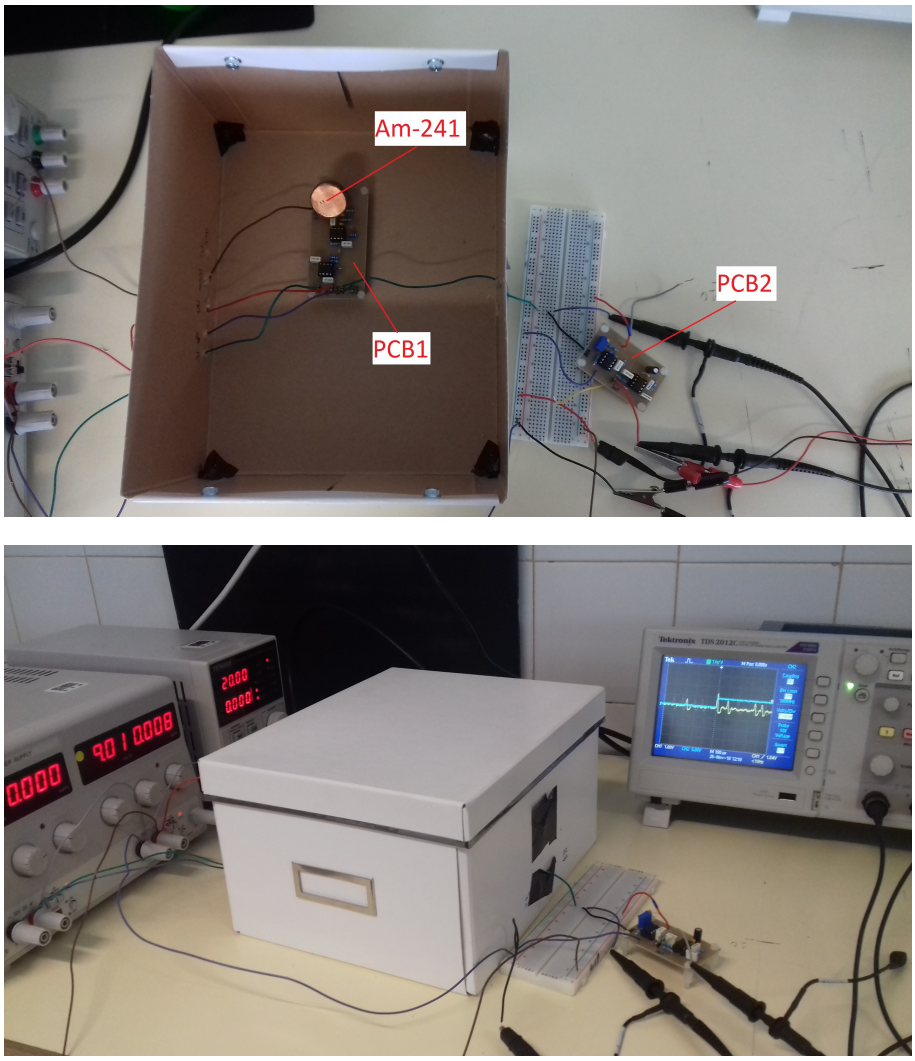

Figure 4.6: Experimental setup for testing the printed circuit boards. The PCB1 has the sensor, preamplifier and amplifier modules. The PCB2 has the discriminator and timer modules.

The Arduino code uses an infinite loop where the most action is programmed. For an external signal to gain control an interrupt to the microcontroller must be made. For this operation, some Arduino pins are provided. The electric circuit output is then connected to digital pin 2 on the Arduino board. We configured by software this pin to behave like an input using ”pinMode()” function.

The signal reaching the Arduino is a square impulse. The transition of a state from LOW to HIGH means one interaction on the photodiode, and consequently one more count. When one of these signals arrive at Arduino’s pin 2, an interrupt to the microcontroller is made and a state variable changes value (from LOW to HIGH). The operation is set by software to happen when the signal is rising.

To count the number of detected impulses, the state variable is checked in the Arduino loop routine. The count variable stores the number of impulses detected at 10 minutes intervals. After this reading time, results are displayed and the variable count is reset.

To set the acquisition time we used the function ”millis()”, that returns the number of milliseconds

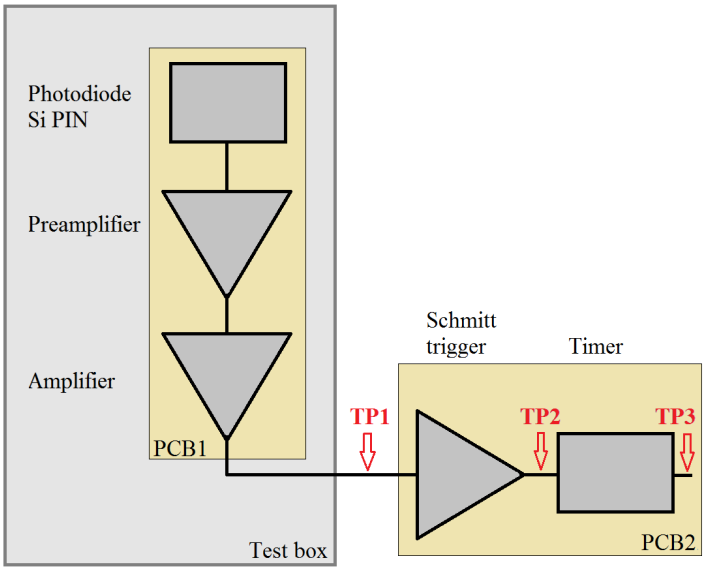

Figure 4.7: Block diagram representative of the electrical circuit chain with indication of the three test points (TP).

elapsed since the Arduino board began running the program. After 50 days the time counter overflows and the function millis() resets to zero. However, for our study, it was not relevant since the time acquisition was less than this time.

Finally, to transfer the data from the microcontroller to a text file, we used the free and open source software PuTTY.

4.5 Final radon monitor prototype

4.5.1 Electronics enclosure box

After testing the electrical printed circuit boards we placed and attach them inside a commercial metallic box that would be the final box for the prototype.

We used a commercial diecast aluminum enclosure fabricated by HAMMOND, with size of $22.2 \times 14.5 \times 5.5$ cm^3. The metallic box will provide good stability, mechanical protection and electromagnetic shielding of the circuits inside.

This enclosure was adapted for the design features pretended. Holes were drilled on the box side for the gas radon to enter (Figure 4.8(a)). To prevent that the sensor was hit by external light, we painted the interior with black matte paint (Figure 4.8(b)), and stick cardboard to the box in labyrinth format. The box has one rubber over the top that blocks light leaks between the lid and the box. The Arduino was placed on the opposite side of the sensor since it has a bright led during acquisition. Figures 4.8 and 4.9 show the adapted box and the interior of the final radon monitor prototype developed.

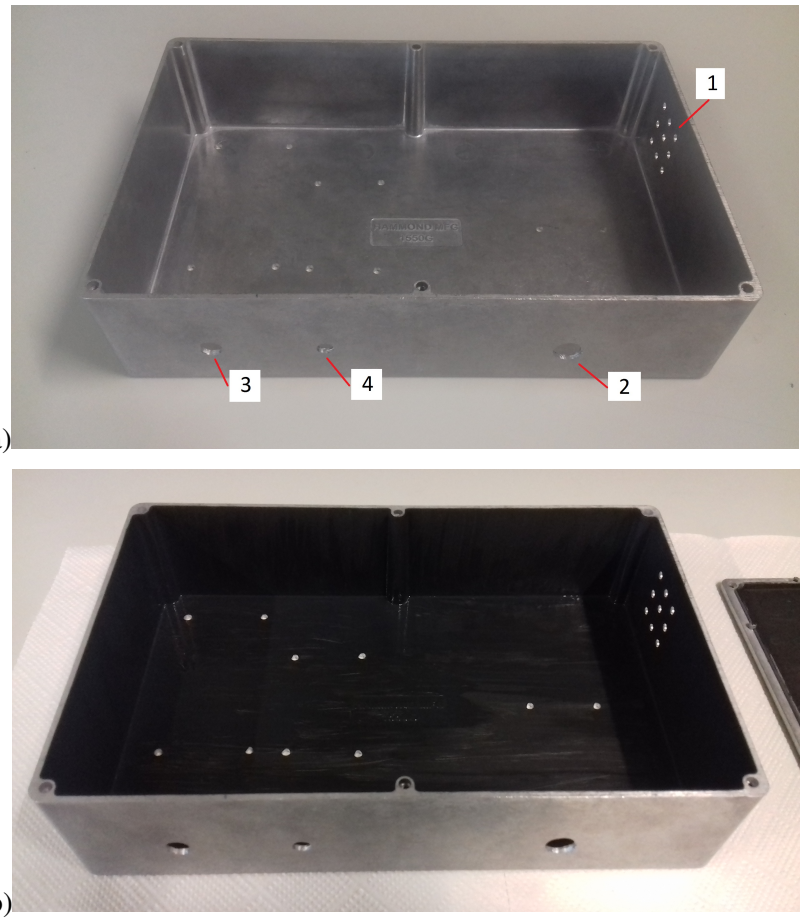

Figure 4.8: Adapted aluminium box for the final radon monitor prototype. (a) Drilled holes (1) for radon gas entry, (2) for the Arduino cable, (3) for sensor bias supplying, and (4) for electric circuit bias supplying. (b) Painted box.

4.5.2 Test of the final radon monitor prototype

The final prototype was tested under laboratory conditions where the radon atmosphere was provided by a box with rock samples. These rocks are from a uranium mine located in the municipality of Nisa, Portugal. The gas diffuses through a tube to a plastic box (test chamber) where all the diverse detectors have been placed. The gas tube is connected to two valves one on each box. During the irradiation tests, the test chamber was kept sealed as possible to prevent radon gas leaking. The monitor was connected to a computer for data acquisition, and the signals from the amplifier output and the timer output were also visualized using an oscilloscope.

We started by studying how the variation of the reverse bias applied to the photodiode affect the detector's response. For this propose we placed the prototype inside the test plastic box and changed the polarization from -9 V to -15 V, and -20 V. This was carried out in continuous acquisitions and the gas admission valves were kept open at all time. The irradiation time was about 5 days. After this time the valves were closed and the test box opened.

Finally, we set the experimental setup to carry out a final long-time acquisition experiment also in a rich radon atmosphere. The reverse bias applied to the sensor was kept constant at -18V. In this exper-

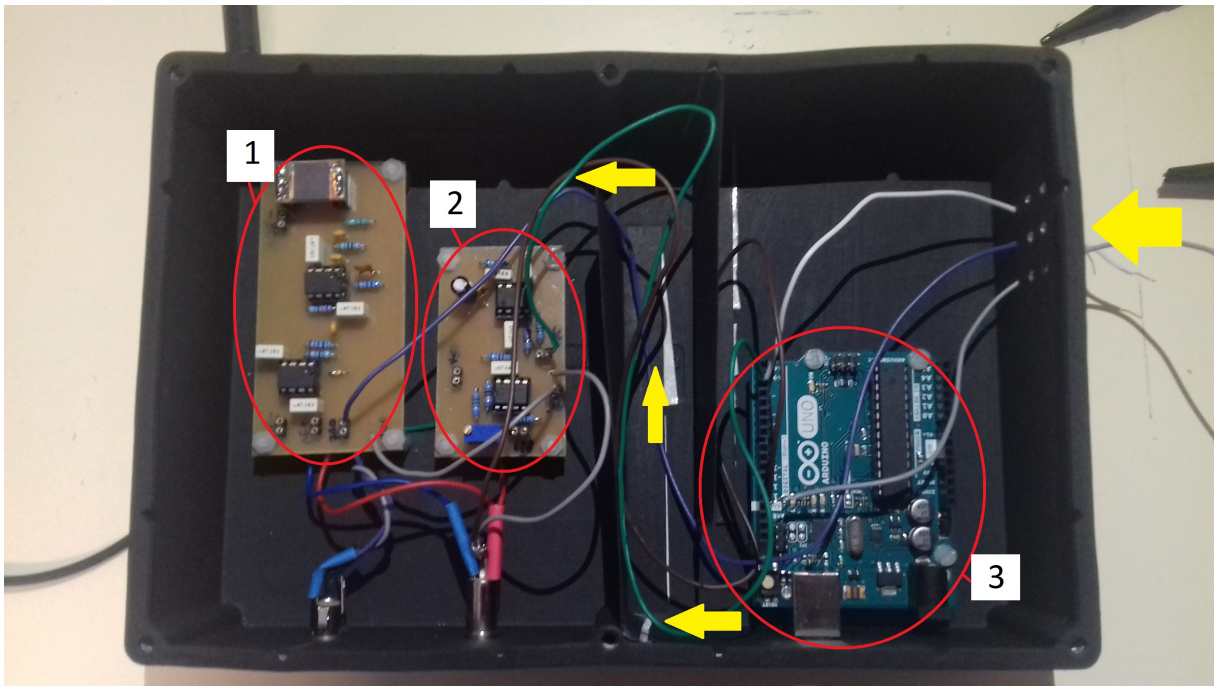

Figure 4.9: Final radon monitor prototype. (1) PCB1 with the sensor, pre-amplifier and the amplifier modules. (2) PCB2 with the trigger and timer modules. (3) Arduino UNO board. The yellow arrows illustrate the movement of the radon gas into the box.

iment parameters as air room temperature and barometric pressure were continuously measured using a BME280 sensor with acquisition through an Arduino UNO microcontroller [47]. The chamber was closed and sealed, the valves were opened again. Because of an electricity break down, an interruption in the acquisition of data was made and continued the following day without closing the valves. The total irradiation time was about 1 month.

To evaluate the behavior of the prototype in continuing acquisition a Geiger Muller detector (GM-10) was also placed inside the plastic test box and connected to a computer. For reading and storing data, we used the provided Rad software.

The GM-10 is a small and simple detector, connected to a computer and supplied by USB. It operates as a pulse counter, without energy resolution. This makes it a favorable choice as a comparable detector to compare our prototype, in a continuous type acquisition. Figure 4.10 shows the implemented setup.

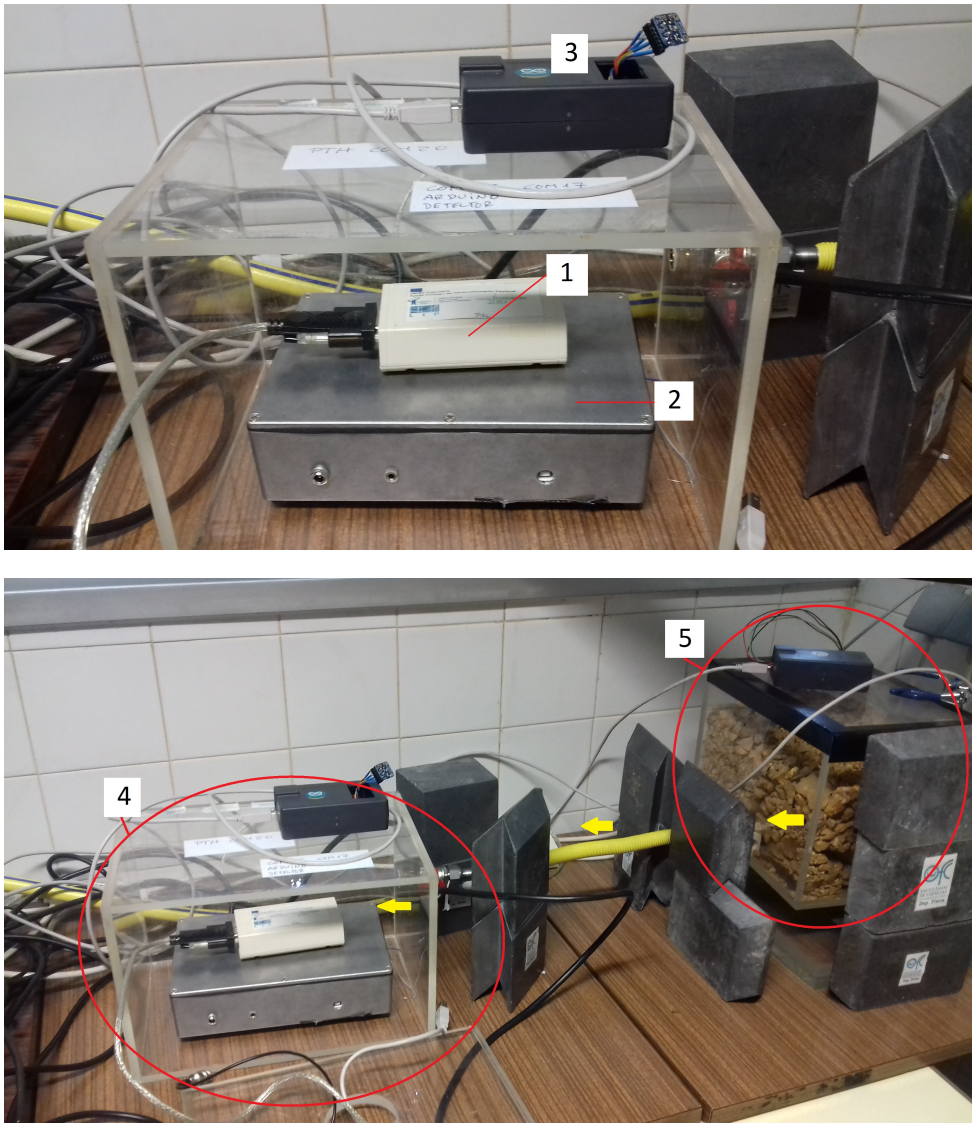

Figure 4.10: Experimental setup for testing the radon detector final prototype system. (1) Geiger Muller detector GM-10. (2) Final radon monitor prototype. (3) Temperature and pressure sensor. (4) Plastic test chamber. (5) Radon source box. The yellow arrows illustrate the movement of the radon gas from the radon source box into the test chamber through a gas tube.

Chapter 5

Results and discussion

5.1 Testing the printed circuit boards

To test the circuit we irradiated the SiPIN sensor with alpha particles from a $^{241}\mathrm{Am}$ source and measured the voltage response at three different points on the circuit. Test point one (TP1) corresponds to the amplifier output, test point two (TP2) to the trigger output, and test point three (TP3) to the timer output (Figure 5.1). Signals at the output of the preamplifier were not observable by oscilloscope because of the noise signal.

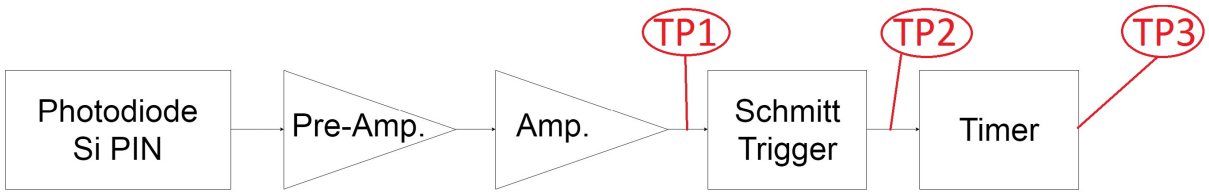

Figure 5.1: Block diagram representative of the electrical circuit chain with indication of the test points.

Figure 5.2 shows the signal observed at TP1 in absence of incident charged particles. Since its amplitude, about 100 mV, was lower than trigger threshold, no signal was observed at TP2 and TP3. The measurement of this signal amplitude, mostly noise, was important to get a reasonable future threshold value.
Figures 5.3 and 5.4 show the signals observed at TP1, TP2 and TP3 obtained placing the $^{241}\mathrm{Am}$ source above the photodiode.
At TP1 we observed pulses with amplitude in a range from 400 mV to 1.8 V. When the height of these pulses were sufficient to set the trigger on, signals were observed at TP2 and TP3.
As we can see the signal from TP1 is a positive pulse whose amplitude is much higher than the noise. So thanks to the presence of these signals, which appear when we place the source, we can identify them as the interactions of charged particles in the photodiode.

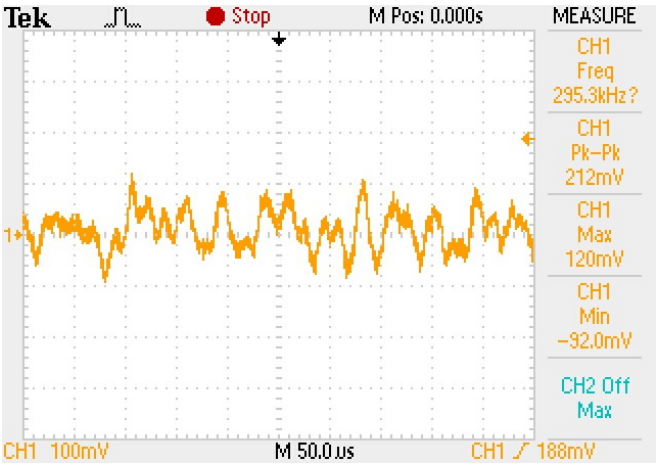

Figure 5.2: Typical amplifier output signal without a radioactive source near the photodiode.

Figure 5.3: Output signals with the radioactive source $^{241}\mathrm{Am}$ placed on the top of the photodiode. The orange line is the one observed at TP1 when a charged particle strikes the sensor and the blue line is the associated square output signal observed at TP2.

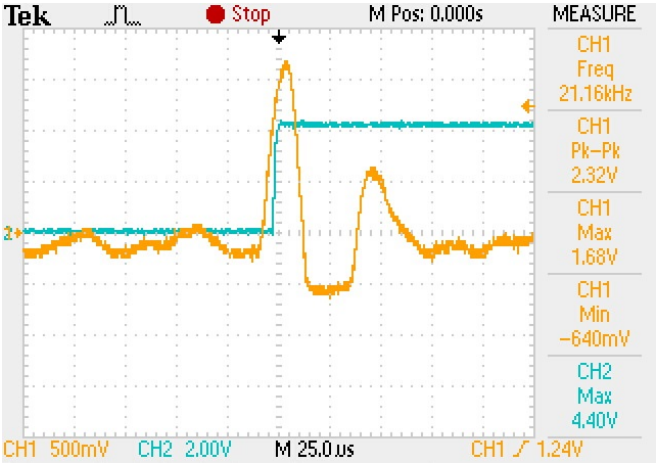

Figure 5.4: Output signals with the radioactive source $^{241}\mathrm{Am}$ placed on the top of the photodiode. The orange line is the one observed at TP1 when a charged particle strikes the sensor and the blue line is the associated square output signal observed at TP3.

5.2 Test of the final radon monitor prototype

Figure 5.5 shows the measurement results of the prototype device for three different values of polarization voltage. The obtained results are compared with the measurements of a Geiger Muller detector (GM-10) placed in the same radon environment. Each experimental dot corresponds to the sum of counts acquired in a ten-minute interval.

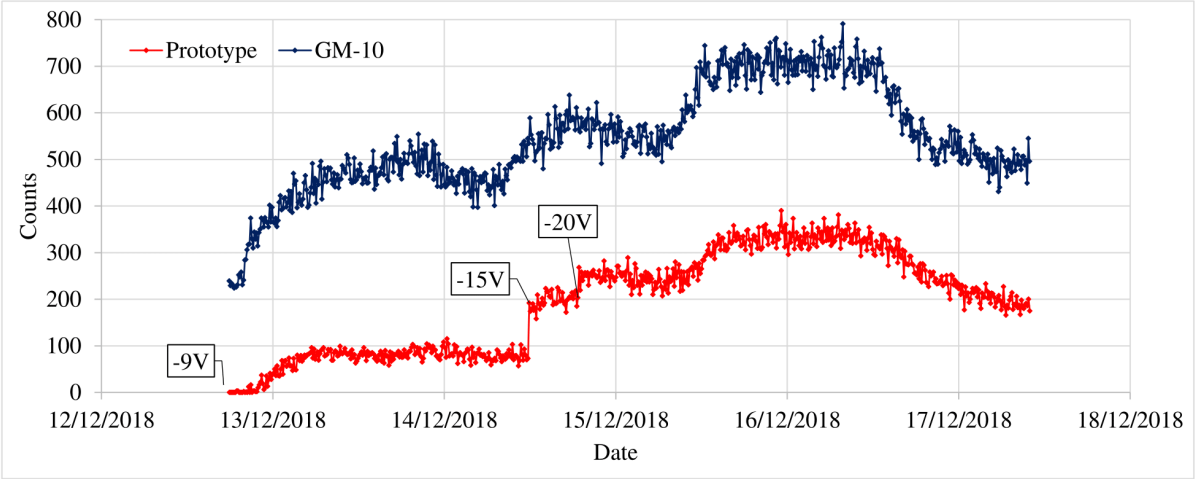

Figure 5.5: Counts of prototype and GM-10 detector during five days of radon continuous exposure. To the former we changed the polarization voltage applied to -9 V, -15 V and -20 V.

When we compare the results from the prototype with the GM-10 detector, we can observe some differences. First, with the applied voltage of -9 V, it was possible to observe a progressive increase in the number of counts that we identified as to be the initial filling of the radon test chamber. However, it did not show sufficient sensitivity to detect radon level fluctuations detected by the GM-10. When biased at -15 V we can see an increase in the number of counts but a sufficient acquisition was not made that we could see the evolution in time since we took the option of pushing the voltage to the limit allowed by the photodiode. Lastly, with the applied voltage of -20 V the sensitivity of our detector increases and a good correlation with the GM-10 detector is obtained being possible to observe the radon level fluctuations.
So the detection response shown to be affected by the polarization applied to the sensor, increasing the sensitivity of the detector with the increase of the reverse voltage. In a way, this effect may be due to the increase of the electrostatic attraction or due to a larger collection of charges in the depletion junction of the photodiode.
Since we placed a large resistor, as a protection of the photodiode, a high drop of voltage is made across the resistor and the actual polarization voltage applied to the photodiode is, in fact, lower than the supplied voltage. We used a 100 MΩ resistor and the actual biased for -9 V, -15 V, and -20 V corresponds to about -4 V, -7 V and -9 V, respectively. On a future version of the circuit, the value of this resistor could be updated to a lower value.

Figure 5.6 shows the raw data of the long-time acquisition experiment in order to test the performance of the final prototype device. The polarization voltage was set to -18 V, then about -8 V applied to the photodiode. We compare the results with those from a commercial Geiger Muller GM-10 detector. Each experimental dot corresponds to the sum of counts acquired in a ten-minute interval and clearly presents the presence of radon inside the test chamber. The acquisition time was from December 18th to January 14th. Simultaneously measurements of air room temperature and barometric pressure were also taken.

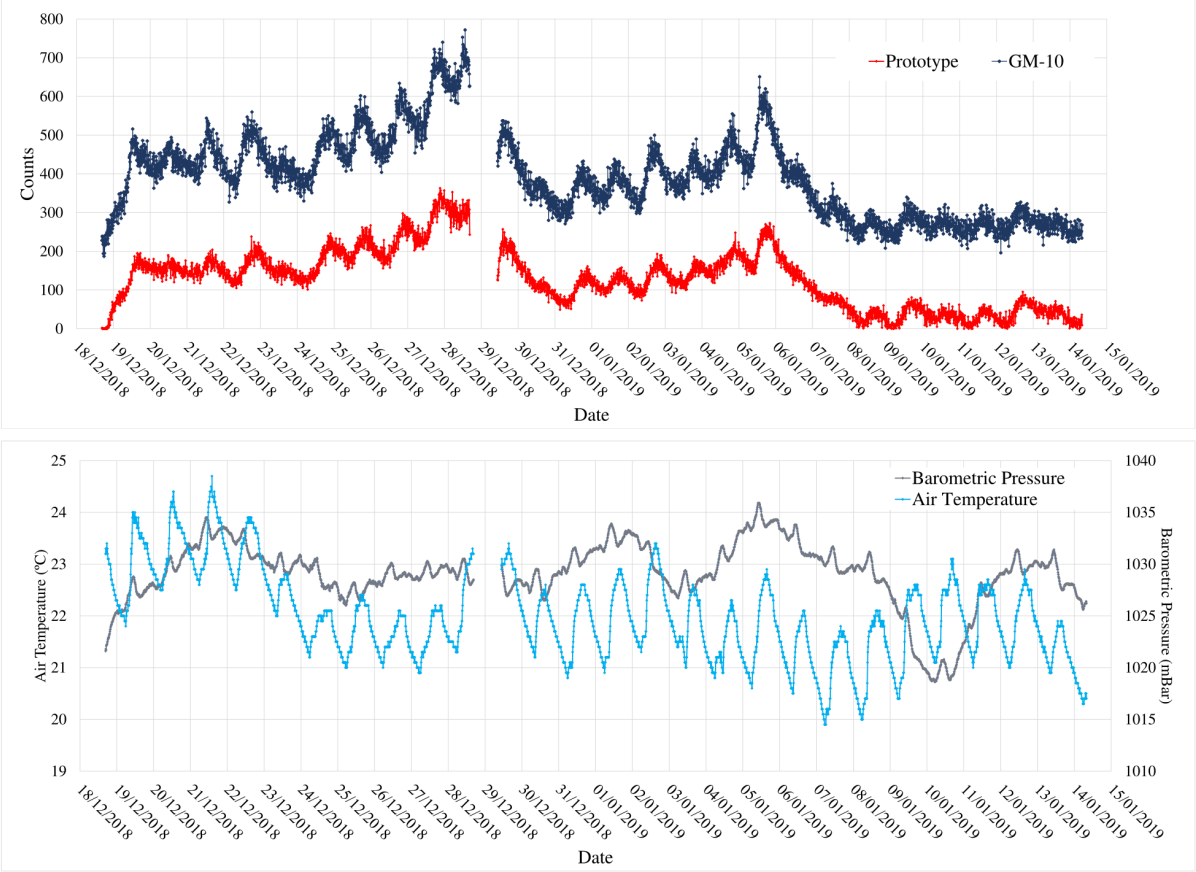

Figure 5.6: The upper graph presents the time-series obtained from the radon measurements with the prototype and the GM-10 detectors. The lower graph presents the air room temperature and barometric pressure measured at the same time.

To evaluate the association between the number of counts acquired with the developed prototype and the number of counts acquired with the commercial Geiger Muller a Pearson correlation test was made. For both raw data presented in the upper graph, a sum of counts was made every hour over the acquisition period.

Figure 5.7 shows a high positive correlation ($n = 622, r^2 = 0.96$) between the data of our detector and those of the counter GM-10. This means that when the number of counts measured by the GM-10 increases, the number of counts measured by the prototype increases as well.

Note that despite having made these measurements with a low bias voltage applied to the Si-PIN, the

results are quite satisfactory. This shows that it is possible to make our device work on batteries only.

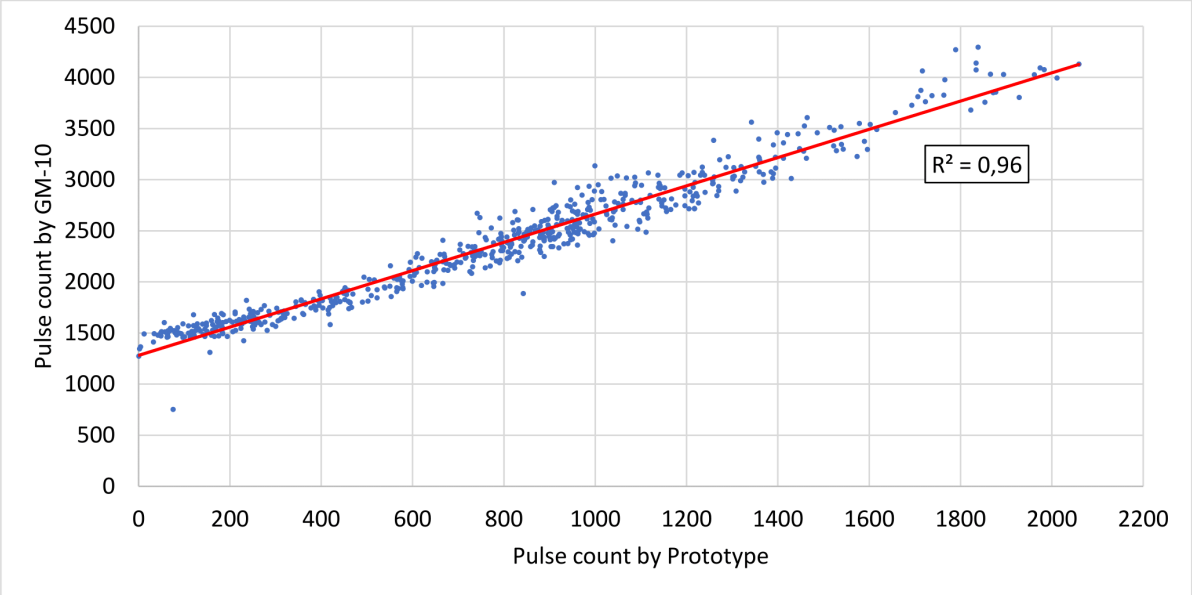

Figure 5.7: Correlation between the sum of counts acquired in an hour interval by the prototype and the Geiger Muller GM-10.

From the upper graph on the figure 5.6 we can also observe daily fluctuations correlated with the daily fluctuations of ambient air temperature evident in the lower graph on the figure 5.6. These diurnal variations vary by about a factor of two with higher total counts during the night than during the day, being in agreement with studies of several authors [3].

The increase of radon flux was also expected for a decrease in the barometric pressure, but looking to the results an obvious negative correlation between the two variables cannot be observed [48, 49].

Since in the first few hours of measurements, there was no evidence of radon inside the test chamber, it was possible to estimate the number of counts due to background radiation. The number of counts due to the background radiation for the developed prototype is about 2 counts and for the Geiger detector about 200 counts.

We can also estimate the acquisition time required to evaluate a site with an uncertainty on the radon concentration. In the characterization of the radon source chapter, we present an experiment where is estimated the order of magnitude of radon concentration achieved over 16 h inside the 10 L test chamber using a NaI(Tl) scintillation detector. The radon concentration was about 100 kBq/m^3. From the prototype's measurements, we obtained an average of 1000 counts per hour. We then presume that corresponds to a overall radon concentration obtained with the NaI(Tl). So, if we intend to make measurements on a site with 100 Bq/m^3, and taking into account uncertainties of about 10-20%, the estimated acquisition time necessary to have the required data statistics is about 4 days to 1 day respectively.

Chapter 6

Conclusions

In this work, we developed and tested a prototype of an active radon detector in air based on a commercial silicon PIN photodiode working in counter mode. It is remarkable that the detector has a low fabrication cost, but still, it has a good performance for alpha particle detection. The components have a fair price and are easy to obtain making the detector very accessible. In fact, the way it was designed makes it cheap and reproducible.

We focused only on the design of a circuit that simply counts the pulses generated by the charged particles hitting the sensor. The photodiode used as the main sensor was the SLCD-61N5 with an active area of 9.67×9.67 mm^2, and cost of only a few euros. The signal generated by the sensor fed an electronic circuit composed of a preamplifier, an amplifier, a discriminator, a timer and a common microcontroller Arduino UNO connected to a computer for data acquisition.

A container with rocks collected at a uranium mine located in Nisa, Portugal, provided the radon atmosphere used in the experiments. Some preliminary experiments were made to estimate the radon concentration from these rocks.

The first experiment present is simultaneous irradiation of solid-state nuclear track CR-39 type detectors and a commercial semiconductor Ramon 2.2 detector. The test chamber (4.5 L) was connected to the source through a gas tube. We found radon concentrations of about 3.4 kBq/m^3 and 2.3 kBq/m^3 for CR-39 and Ramon 2.2 respectively. The deviations can be justified in a way due to the generic calibration factor supplied by the manufacturer used to calculate the concentration values for the CR-39. Using calibrated CR-39 detectors are fundamental if a reliable comparison is desirable. This process was not achieved because it was out of our laboratory instrumentation possibilities.

With the CR-39 data results, we also present a new method to count alpha-tracks using the free software CellProfiler. We compared the results with those obtained by visual tracks counting. Reasonable deviations of about 1-14% were found. We can say that this method provides a very easy and inexpensive way to analyse nuclear track detectors. However, it should be noticed that when analysing bare images

the software may give an unrealistic number of tracks.

Another way to estimate the concentration of radon in air is suggested by gamma radiation detection using a sensitive 2"×2" sodium iodide scintillation detector. The irradiation was carried out in a test chamber with 10 L of volume. We found a radon concentration of about 10^5 Bq/m^3.

Before testing the prototype in a rich radon air atmosphere, the operability of the detector was proven using a radioactive source. As we wanted to detect alpha particles from radioactive decay of radon and its progeny whose energies range from 6.0 to 7.7 MeV, we choose an $^{241}\mathrm{Am}$ alpha-emitting source, with energy of 5.5 MeV, assumed to be sufficient for the test. The test was implemented with the sensor board inside a closed light-tight box. The signals were measured by an oscilloscope at the amplifier's, trigger's and timer's outputs. In the absence of the radioactive source, signal with an amplitude of about 100 mV was observed and considered as electronic noise. In presence of the radioactive source above the surface of the photodiode, pulse signals with a range of amplitude from 400 mV to 1.8 V were observed and considered as due to the hits of charged particles.

Established the operation of the detector for alpha radiation, we performed experiments in an radon gas atmosphere. A commercial metallic box was adapted to enclose the sensor and the electronics. Holes were drilled to make a way for the gas to diffuse into the box. To prevent the light to hit the sensor, the inside of the box was painted with black matte paint and a cardboard in labyrinth format placed inside.

The source box was connected through a gas tube to a 10 L test chamber, where the detectors were placed. The system did not have a gas pumping system, so when the valves were kept open for a while, the radon gas mixed with air diffused by concentration gradient into the test chamber.

The thresholds set to reject noise were experimentally adjusted taking into account the amplitude of noise and the signals of greater amplitude previously mentioned. For measurements in radon air atmosphere this level was set at 680 mV, a lower value than the one used in the test with the americium source. The aim was to detect pulses with amplitude slightly lower than expected. The reason why we observed lower amplitude pulses is possible due to the significant loss of energy as a result of interaction with air through which incident particles must pass before reaching the sensor. In order to better estimate this level, it could be done if the energy spectrum was available.

From the radioactive radon series, polonium, lead and bismuth ions are also produced. For example, $^{218}\mathrm{Po}$ ions are charged positively due to the stripping of orbital electrons by the departing alpha particles in the recoil motion, about 80% of these maintain their charge, and the remain may become neutralized [19]. As a result, detectors working with electrostatic deposition have been developed by many authors for detection of radon through their charged decay products [27–32].

With this in mind, we studied how the variation of the reverse bias voltage applied to the sensor affected the detection response. We varied the reverse bias applied from -9 V to -15 V, and -20 V. The results

were compared with the measurements of a commercial Geiger Muller GM-10 placed in the same radon environment. From this study, was observed that the detection response is affected by the polarization applied to the sensor, increasing the sensitivity of the detector with the increase of the reverse voltage. In a way, this effect may be due to the increase of the electrostatic attraction or due to a larger collection of charges in the depletion junction of the photodiode. Experiments to differentiate these two facts should be conducted in the future.

Despite the low bias voltage, in all cases it was possible to detect pulses since the deposited energy was high enough to generate pulses above the electronic noise.

Finally, a long-term acquisition was performed during about one month, also in a radon gas atmosphere, with an applied polarization voltage of -18 V. We obtained a high positive correlation between the results from the prototype and the GM-10 achieving the main goal of this work.

Parameters as air temperature and barometric pressure were continuously measured as well, and from this data, we could correlate the daily counts fluctuations with the daily temperature fluctuations, mentioned by [3]. However, no evident correlation between our results and the barometric pressure was found.

From the first hours of acquisition we estimate the number of counts as result of background radiation to be about 2 counts for the developed prototype and 200 counts for the Geiger counter.

Using the results from the characterization of the radon source provided by the gamma rays detection, we estimate the time exposure required to perform measurements with different radon levels. For example for about 100 Bq/m^3 it is estimated that the prototype will take about 4 days to 1 day for uncertainties of 10% to 20% respectively.

The use of a Geiger Muller as the instrument chosen to cross-check the results from the developed prototype, had the advantage to visualize in real time the behavior of the detector. However, information about the radon concentration during the acquisition time was not obtained, since the Geiger only provide values in counts as it is not calibrated for radon detection.

We propose to use a scintillation detector of NaI(TI) in order to have a measure of comparison in radon concentration with the results of our prototype in real time. Simultaneous exhalations should be performed in the future.

In short, we also suggest the possibility to make our detector totally portable working powered only by batteries, and using a memory card shield attached to the Arduino to store the data. This new design will allow to operate in areas where electricity supply is not stable.

Bibliography

[1] UNSCEAR. *Sources and effects of ionizing radiation: sources*, volume 1. United Nations Scientific Committee on the Effects of Atomic Radiation publications, 2000. ISBN 92-1-142238-8.

[2] UNEP. *Radiation: Effects and Sources*. United Nations Environment Programme, 2016. ISBN 978-92-807-3517-8.

[3] C. R. Cothern and J. E. Smith Jr. *Environmental Radon (V. 35)*. Springer Science & Business Media, 2013. ISBN 978-1-4899-0475-1. Doi:10.1007/978-1-4899-0473-7.

[4] NIST. *Atomic Weights and Isotopic Compositions for Radon*. National Institute of Standards and Technology, accessed 6 October 2018. `https://physics.nist.gov/cgi-bin/Compositions/stand_alone.pl?ele=Rn&isotype=all`.

[5] CIAAW. *Isotopic Compositions of the elements 2017*. Commission on Isotopic Abundances and Atomic Weights, accessed 6 October 2018. `http://www.ciaaw.org/isotopic-abundances.htm`.

[6] S. Chu, L. Ekstrom, and R. Firestone. *Table of Radioactive Isotopes. Nuclide search Z=86*. The Lund/LBNL Nuclear Data Search (V 2.0), accessed 6 October 2018. `http://nucleardata.nuclear.lu.se/toi/listnuc.asp?sql=&Z=86`.

[7] Y. Ishimori, K. Lange, P. Martin, Y. Mayya, and M. Phaneuf. *Measurement and calculation of radon releases from NORM residues*. IAEA, 2013.

[8] WNA. *Geology of Uranium Deposits*. World Nuclear Association Website, accessed 11 November 2018. `http://www.world-nuclear.org/information-library/nuclear-fuel-cycle/uranium-resources/geology-of-uranium-deposits.aspx`.

[9] IAEA. *World Distribution of Uranium Deposits*. International Atomic Energy Agency, accessed 11 November 2018. `https://www-pub.iaea.org/books/IAEABooks/12314/World-Distribution-of-Uranium-Deposits-Second-Edition`.

[10] M. Baskaran. *Radon: A tracer for geological, geophysical and geochemical studies*. Springer, 2016.

[11] NCRP. *Measurement of Radon and Radon Daughters in Air: Recommendations of the National Council on Radiation Protection And Measurements (Report No. 97)*. 1988. ISBN 0-913392-97-9.

[12] ATSDR. *Toxicological profile for radon*. United States Department of Health and Human Services: Agency for Toxic Substances and Disease Registry, 2012.

[13] J. H. Lubin, J. D. Boice Jr, C. Edling, R. W. Hornung, G. R. Howe, E. Kunz, R. A. Kusiak, H. I. Morrison, E. P. Radford, J. M. Samet, et al. Lung cancer in radon-exposed miners and estimation of risk from indoor exposure. *JNCI: Journal of the National Cancer Institute*, 87(11):817–827, 1995.

[14] D. Laurier. *Progress in understanding radon risk*. Institute for Radiological Protection and Nuclear Safety, 2010. EU Scientific Seminar 2010 "Issues with internal emitters" Luxembourg, 23 November 2010.

[15] J. M. Samet. Indoor radon and lung cancer. estimating the risks. *Western journal of medicine*, 156 (1):25, 1992.

[16] UNSCEAR. *Sources and effects of ionizing radiation: Report to the General Assembly (Scientific Annex D)*. United Nations Scientific Committee on the Effects of Atomic Radiation publications, 2016. ISBN 978-92-1-142316-7.

[17] UNSCEAR. *Sources, Effects and Risks of Ionizing Radiation: Report to the General Assembly (Scientific Annexes A and B)*. United Nations Scientific Committee on the Effects of Atomic Radiation publications, 2017. ISBN 978-92-1-142322-8.

[18] WHO. *WHO Handbook on Indoor Radon: A public health perspective*. World Health Organization, 2009. ISBN 978-92-4-154767-3.

[19] J. Porstendörfer, P. Pagelkopf, and M. Gründel. Fraction of the positive $^{218}\mathrm{Po}$ and $^{214}\mathrm{Pb}$ clusters in indoor air. *Radiation protection dosimetry*, 113(3):342–351, 2005.

[20] NCR. *The Multi-Agency Radiation Survey and Site Investigation Manual (MARSSIM) NUREG-1575, Rev 1*. United States Nuclear Regulatory Commission, 2000.

[21] D. Al-Azmi, A. O. Mustapha, and N. Karunakara. Radon adsorbed in activated charcoal: A simple and safe radiation source for teaching practical radioactivity in schools and colleges. *Physics Education*, 47(4):471, 2012.

[22] Radosys. Radosys user's manual: Radosys technical specification, revised at 2013.

[23] C. Liu, H. Ma, Z. Zeng, J. Cheng, J. Li, and H. Zhang. Measurements of radon concentrations using CR-39 detectors in China JinPing Underground Laboratory (2015-2016). *Cornell University*, 2018.

[24] M. Budinich and M. Vascotto. The 'radon school survey': Measuring radioactivity at home. *Science in School*, 14:54–57, 2010.

[25] Intercast Europe. Data-sheet: CR-39 Solid State Nuclear Track Detectors.

[26] Black Cat Systems Website. Data-sheet: GM-10 Geiger Counter Radiation Detector, accessed 21 February 2019. `https://www.blackcatsystems.com/GM/products/GM10GeigerCounter.html`.

[27] Y. Takeuchi, K. Okumura, T. Kajita, S. Tasaka, H. Hori, M. Nemoto, and H. Okazawa. Development of high sensitivity radon detectors. *Nuclear Instruments and Methods in Physics Research Section A: Accelerators, Spectrometers, Detectors and Associated Equipment*, 421(1-2):334–341, 1999.

[28] A. Martin-Martin, J. Gutiérrez-Villanueva, J. Munoz, M. Garcia-Talavera, G. Adamiec, and M. Iniguez. Radon measurements with a pin photodiode. *Applied radiation and isotopes*, 64 (10-11):1287–1290, 2006.

[29] C. Mattone. *Development of radon and thoron concentrations measurement techniques with electrostatic collection*. PhD thesis, University of Studies of Naples, 2014.

[30] E. Choi, M. Komori, K. Takahisa, N. Kudomi, K. Kume, K. Hayashi, S. Yoshida, H. Ohsumi, H. Ejiri, T. Kishimoto, et al. Highly sensitive radon monitor and radon emanation rates for detector components. *Nuclear Instruments and Methods in Physics Research Section A: Accelerators, Spectrometers, Detectors and Associated Equipment*, 459(1-2):177–181, 2001.

[31] M. Voytchev, D. Klein, A. Chambaudet, and G. Georgiev. The use of silicon photodiodes for radon and progeny measurements. *Health physics*, 80(6):590–596, 2001.

[32] A. Chambaudet, D. Klein, and M. Voytchev. Study of the response of silicon detectors for alpha particles. *Radiation measurements*, 28(1-6):127–132, 1997.

[33] T. N. Tomo Nakajima. Radiation education with radon detector: Detector development and implementation at high school. 11th International workshop on the geological aspects of radon risk mapping. University of Tsukuba.

[34] G. F. Knoll. *Radiation detection and measurement*. Wiley India Pvt. Ltd., 2009.

[35] HAMAMATSU. *Opto-semiconductor Handbook: Si detectors for high energy particles (Chapter 10)*. accessed 11 November 2018. https://www.hamamatsu.com/sp/ssd/doc_en.html.

[36] OSI-Optoelectronics. *Photodiode Characteristics and Applications: A detailed discussion of silicon photodiodes construction, operation and characteristics*. accessed 11 November 2018. http://www.osioptoelectronics.com/technology-corner/application-notes.aspx.

[37] GT-Analytic. Ramon 2.2 radon monitor. Applications, measurement modes, technology and quality, revised at 2016.

[38] A. E. Carpenter, T. R. Jones, M. R. Lamprecht, C. Clarke, I. H. Kang, O. Friman, D. A. Guertin, J. H. Chang, R. A. Lindquist, J. Moffat, et al. Cellprofiler: Image analysis software for identifying and quantifying cell phenotypes. *Genome biology*, 7(10):R100, 2006.

[39] Cellprofiler Manual: Module IdentifyPrimaryObjects, accessed 12 July 2018. http://d1zymp9ayga15t.cloudfront.net/CPmanual/IdentifyPrimaryObjects.html.

[40] P. Horowitz and W. Hill. *The art of electronics*. Cambridge Univ. Press, 1989.

[41] ORTEC. Preamplifier introduction, accessed 23 February 2019. https://www.ortec-online.com/-/media/ametekortec/other/preamplifier-introduction.pdf?la=en.

[42] Texas-Instruments. Data-sheet: LF442-MIL Dual Low Power JFET Input Operational Amplifier, revised at 2017.

[43] Texas-Instruments. Data-sheet: LM111, LM211, LM311 Differential Comparators, revised at 2017.

[44] Texas-Instruments. Data-sheet: LM555 Timer, revised at 2015.

[45] Arduino-Website. *Arduino UNO REV3: Tech specifications*. accessed 24 February 2019. https://store.arduino.cc/arduino-uno-rev3.

[46] S. Chu, L. Ekstrom, and R. Firestone. *Table of Radioactive Isotopes:* $^{241}\mathrm{Am}$. The Lund/LBNL Nuclear Data Search (V 2.0), accessed 24 February 2019. http://nucleardata.nuclear.lu.se/toi/nuclide.asp?iZA=950241.

[47] Adafruit-Industries. *BME280 Humidity, barometric pressure and temperature sensor*. accessed 24 February 2019. https://cdn-learn.adafruit.com/downloads/pdf/adafruit-bme280-humidity-barometric-pressure-temperature-sensor-breakout.pdf.

[48] S. Schery and D. Gaeddert. Measurements of the effect of cyclic atmospheric pressure variation on the flux of 222rn from the soil. *Geophysical Research Letters*, 9(8):835–838, 1982.

[49] H. Zafrir, S. M. Barbosa, and U. Malik. Differentiation between the effect of temperature and pressure on radon within the subsurface geological media. *Radiation Measurements*, 49:39–56, 2013.

Appendix A

Arduino data acquisition code

```
/*****************************************************************
                    RADON COUNTER
*****************************************************************/

float timer = 600.;
const byte interruptPin = 2;
volatile byte state = LOW;
unsigned long counter = 0;
unsigned long time0 = 0.;
unsigned long totaltime;
float         dt = 0;

void setup() {

  Serial.begin(9600);
  pinMode(interruptPin, INPUT);
  attachInterrupt(digitalPinToInterrupt(interruptPin), interr, RISING
     );
  time0 = millis();
  Serial.println("START");

}


```

```
24 void loop() {
25   if(state == HIGH) {
26   state = LOW;
27   counter++;
28   delayMicroseconds(10000);
29   }
30
31   dt = (millis()-time0)/1000.;
32
33   if( dt >= timer) {
34     Serial.print("time(s):"),Serial.print(millis()/1000.),Serial.
         print("counts:"), Serial.println(counter);
35     time0 = millis();
36     counter = 0;
37   }
38
39 }
40
41 void interr() {
42
43   state = HIGH;
44
45 }
```